GS-MBE GROWTH OF Ga(In)AsN NITRIDES FOR LONG WAVELENGTH SEMICONDUCTOR LASERS

GS-MBE GROWTH OF Ga(In)AsN NITRIDES FOR LONG WAVELENGTH SEMICONDUCTOR LASERS

By
Lixiang Yuan, B.Eng., M.Eng.

A Thesis
Submitted to the School of Graduate Studies
in Partial Fulfillment of the Requirements
for the Degree
Master of Engineering

McMaster University

Master of Engineering (2000) McMaster University
Engineering Physics Hamilton, Ontario

TITLE: GS-MBE growth of Ga(In)AsN nitrides for long wavelength semiconductor lasers

AUTHOR: Lixiang Yuan, B.Eng. (Tianjin University, China)
M.Eng. (Chinese Academy of Science, China)

SUPERVISOR: Prof. David A. Thompson

NUMBER OF PAGES: x, 97

ABSTRACT

Quaternary GaInAsN containing a small amount of nitrogen (<2%) is a potentially promising material for realizing long wavelength emission lasers for applications in optical communication systems. Such devices should have better high temperature characteristics than conventional InGaAsP lasers due to an increase of the conduction band offset. In this thesis, the GS-MBE growth of quaternary GaInAsN and ternary GaAsN were carried out. Active N was produced by passing high purity nitrogen gas into either a RF or an ECR plasma source. The RF plasma source was found to produce better quality nitrides. Characterization techniques such as photoluminescence, X-ray diffraction, TEM, SIMS, and Hall effect measurements were used to characterize thick layers (e.g. 1 μm) and quantum wells of these nitride materials.

The concentration of N incorporated into GaInAs and GaAs is very dependent on growth conditions and plasma conditions. The incorporation of a small amount of N into compressively strained InGaAs reduces the strain and produces a red-shift of photoluminescence peak. However, compared to N-free InGaAs materials, the optical quality is dramatically degraded yielding reduced photoluminescence intensity and a broadened FWHM of the PL peak. Hall effect measurements on un-doped, Si-doped, Be-doped thick GaInAsN layers indicate the presence of a high concentration of electron and hole traps. The results of SIMS suggest that impurity H might be responsible for the deep level defects formed. However, the nature of the defects is currently unknown. From TEM observations and comparison to samples grown with a He-plasma instead of a N-plasma, spinodal decomposition and ion induced damage in GaInAsN may produce reduced quality of materials, but these are not the major reasons responsible for the dramatic degradation of optical quality.

Thermal annealing was found to be an effective method for significantly improving the optical quality of GaInAsN with a low N concentration. Optimum annealing conditions were obtained. Hall effect measurements on annealed samples indicate that electron and hole traps are reduced but still present after anneal.

ACKNOWLEDGEMENTS

I would like to take this opportunity to express my gratitude for the supervision of Dr. David A. Thompson. Special thanks are also deserved by Brad Robinson and Scott McMaster for the GS-MBE growths and characterization of the materials. In particular, I was greatly benefited from the insightful discussions with Brad Robinson. Thanks are also given to Wu, Andy and Fred for the assistance with TEM. SIMS measurements were performed by Richard W. Streater, Nortel Networks. I owe many thanks to my wife Yuhong and my lovely daughter Alice for their support, love and passion.

I would also like to thank my friends and colleagues in my department, Zhilin, Zhendong, Cherry, QC, Kate, Zhaojun, Qiang Liu and Adam. A special thank was given to my soccer team, all-year-round soccer games made my two-years' staying in Hamilton so enjoyable .

Dedicated to my wife Yuhong, and
my daughter Alice

TABLE OF CONTENTS

LIST OF FIGURES

CHAPTER 1
Introduction

It is well known that the semiconductor laser diodes applied in optical communication systems operate in the 1.3 or 1.55μm wavelength ranges to minimize loss in the optical fiber. The most commonly used material systems include InGaAs/InGaAsP/InP and InGaAsP/InP. However, lasers made in these materials systems have poor temperature performance with a typical characteristic temperature, T_0, of ~60K, compared to shorter wavelength 0.98 μm GaAs-based lasers, whose T_0 is over 150K. T_0 is a characteristic temperature often used to express the temperature sensitivity of threshold current. A lower T_0 value implies that the threshold current increases more rapidly with increasing temperature. The high temperature sensitivity of the threshold current of InGaAsP lasers limites their performance under high-temperature operation. Therefore, for stable wavelength emission, thermoelectric coolers are required. There are three factors affecting the high-temperature performance of these long wavelength lasers: (1) poor electron confinement due to the small conduction band offset[1]; (2) Auger recombination[2-4]; and (3) intervalence band absorption[5]. The main reason for the low T_0 is poor electron confinement. Increasing the electron confinement requires increasing the conduction band offset. Thus, for improving the performance of 1.3 μm lasers, alternate materials combinations such as AlGaInAs/InAlAs[7] and InAsP/InGaAsP[8] quantum well (QW) structures have been proposed with demonstrated T_0 values of 120K and 72K, respectively.

M. Kondow and co-workers proposed that a larger conduction band offset could be achieved with a novel mixed group III-V nitride material GaInAsN [9,10]. It is one of

the mixed group III-V nitride alloy semiconductors such as GaPN and GaAsN. GaInAsN can be grown on a GaAs substrate with a bandgap energy suitable for long-wavelength laser diodes. Currently, 1.3 μm is possible and longer wavelength may be possible in the future. By combining GaInAsN with GaAs or AlGaAs, a type-I band alignment is achieved, and quantum wells with a large conduction band offset can be fabricated. This suppresses electron excitation out of the wells into the barrier layers, so it is very attractive for overcoming the poor temperature characteristics of InGaAsP semiconductor lasers. The characteristic temperature of a long wavelength laser using GaInAsN material grown on GaAs substrate is expected to be over 200K.

GaInAsN has potential applications in long wavelength semiconductor lasers with much improved high temperature characteristics. Some demonstration experiments of the fabrication of GaInAsN quantum-well lasers have been reported. With GaInAsN material as the quantum wells, and GaAs as barriers, M. Kondow[9] reported ~1.2 μm emission from a GaInAsN single-quantum-well (SQW) laser with a high characteristic temperature T_0 of 127K. Later, room-temperature pulsed operation of a 1.3 μm GaInAsN/GaAs double-heterostructure laser diode was grown by metal-organic chemical vapor deposition was reported. The nitrogen composition was about ~3%. K. Nakahara[11] reported 1.3 μm lasing action under continuous-wave (CW) operation in the GaInAsN-GaAs SQW laser with nitrogen concentration about 1%. Recently, Li et al[22] reported 1.2 μm GaInAsN three-quantum-well laser diodes grown by organometallic vapor phase epitaxy with the lowest value of threshold current density (J_{th} ~ 1.2KA/cm^2) reported to date. In addition to its use in edge-emitting lasers, GaInAsN has also been used to fabricate vertical cavity surface emitting lasers (VCSEL)[12] with an emission wavelength of 1.18 μm.

In addition to the application in long wavelength semiconductor lasers, other potential applications recently proposed for GaInAsN include solar cells[13,14] and heterojunction bipolar transistors (HBT)[15]. Using the $GaIn_xAsN_y$ alloy system lattice-matched to GaAs with $y \approx 0.35x$, 1eV solar cells have been demonstrated, which may be suitable for the next generations of ultrahigh-efficiency solar cell devices, if the problem with quantum efficiency can be overcome.

Several crystal growth techniques, such as Metalorganic Chemical Vapor Deposition (MOCVD)[16,32]; Gas Source Molecular Beam Epitaxy (GS-MBE)[19,20]; Chemical Beam Epitaxy (CBE)[21]; and Organometallic Vapor Phase Epitaxy (OMVPE)[22] have been succcessfully used to grow GaInAsN. In MOCVD, triethylgallium (TEGa) and trimethylindium (TMIn) are used as group-III source materials, tertiarybutylarsine (TBAs) and dimethylhydrazine (DMHy) are used as group-V source materials. The advantages of TBAs and DMHy compared to the often employed AsH_3 and ammonia, are their low decomposition temperatures which make low temperature growth possible. The relative DMHy flow, $\{x_v$=DMHy/(DMHy+TBAs)$\}$ is a key factor that determines the N content in the GaInAsN layer. The growth temperature is varied between 475^{0}C and 600^{0}C.The growth rate can be around ~1μm/hour. In GS-MBE, metal Ga, metal In, arsine gas, and nitrogen gas are used as precusors. The Ga and In flux was derived from conventional thermal effusion cells. The As_2 flux is obtained by thermal cracking of arsine at 900^{0}C. The N-radical flux is produced by an RF discharge in the N radical cell. The substrate is usually (100)-oriented n-type GaAs and the growth rate is normally 1μm/hour. An AsH_3 flow rate of 1-10sccm, N_2 flow rate of 0.04-1.00sccm, and RF power of 80-500W are typically used. In CBE growth of GaInAsN, TEGa and TMIn are used as group III sources with a hydrogen carrier gas. The arsenic source is 100% arsine precracked at 900^{0}C and the AsH_3 flow was 11sccm in the

experiment. The N radical was again produced by the RF plasma cell with the RF power ranging from 200-300W. The flow conductance of the RF-cell aperture is 50cm^3/s, and the growth temperature is 500^{0}C. To stabilize the radical condition, the RF cell is ignited while the buffer layer is being grown. In the OMVPE reactor, typical substrate rotation speed is 60rpm. Trimethylindium and triethylgallium are used as group III sources, and AsH_3 and DMHy are used as group V sources. The carrier gas is N_2, and SiH_4 and trimethylgallium are used as n- and p-type doping, respectively. The growth temperature is between 500- 535^{0}C. For our work, we make use of GS-MBE as the growth method and have used a variety of nitrogen sources such as thermally dissociated NH_3 and various plasma sources of nitrogen radicals.

The growth of high quality GaInAsN/GaAs quantum wells (QWs) is very difficult, especially for a highly-strained GaInAsN layers with a large In content. This difficulty in the growth of high quality mixed III-V nitride materials may be mainly due to their miscibility gap[16,17,18], which originates from large differences in atomic properties of group-V elements, such as atomic radius and electronegativity[23]. Incorporation of N into GaInAs is very dependent on the growth conditions. The incorporation rate was reported to drop exponentially with increasing growth temperature[25]. The N content is also related to the N_2 gas flow rate, RF power, and AsH_3 flow in gas-source MBE growth[20], while in MOCVD[16,32], the V/III flux ratio was found to be an important parameter for the N composition and photoluminescence intensity. It was also found that the N content in GaInAsN is a function of the In content[28]: as the In content increases, the N content decreases. This decrease in N content is thought to be due to the relatively weak In-N bond, compared to the Ga-N bond, resulting in a larger degree of N desorption.

As the N content increases in GaInAsN, the light emission properties deteriorate. Also, the threshold current density of GaInAsN laser diodes that have been demonstrated[24,26] are relatively high compared with standard InGaAsP laser diodes. Basically, incorporation of N in GaInAsN results in a red shift of photoluminescence peak position, i.e., a reduced bandgap of the crystal, and the net strain is also reduced. However, as the N concentration increases, a reduced photoluminescence emission and a broader linewidth is observed. This could be due to phase separation resulting from the large miscibility gap and associated nonradiative defect centers. In the MOCVD growth of GaInAsN, where the active N is obtained from dimethylhydrazine (DMHy), possible additional reasons for low photoluminescence intensity[28] are (1) increased group-V vacancy concentrations due to the decomposition of In-N bonds, (2) high carbon and/or hydrogen contamination accompanied by the N incorporation, (3) dislocation of In atoms due to migration. If active N is obtained from a plasma source (RF or ECR), such as used in MBE growth, then the ion induced damage from the plasma is a widely used explanation of the poor PL performance of GaInAsN[38]. The defect levels associated with the ion damage may form deep non-radiative recombination centers, quenching the photoluminescence emission. This will be discussed in later chapters in relation to our experiments. There is still much work to be done on the growth and characterization of GaInAsN.

Several ways have been demonstrated to effectively improve the crystal quality and the optical quality of GaInAsN materials. (1) Since N incorporation and photoluminescence intensity of GaInAsN are very dependent on the growth conditions, work has been carried out in an attempt to optimize the growth conditions; i.e., growth temperature, plasma source operation condition and III/V flux ratio of the sources. Also, different plasma sources for producing atomic N and eliminating the N_2^+ ions have been

explored. (2) Post-growth anneals have been shown to remarkably improve the quality of GaInAsN/GaAs QW[16,29,30,31]. This was investigated through changes in the PL properties with increases in the PL intensity by almost two orders of magnitude being achieved. A blue-shift of the PL peak wavelength of GaInAsN/GaAs QWs is observed due to the structural change the QWs. This blue-shift is caused by In-Ga interdiffusion rather than the nitrogen atom diffusion. The interdiffusion caused by defects is thought to reduce the number of non-radiative centers[33,35], resulting in improved PL performance. T. Kitatani et al.[34] demonstrated that an in-situ anneal in the MBE chamber for 1hour at temperatures of 500- 600 ^{0}C under an AsH_3 flow rate of 5 sccm also improved the PL characteristics. (3) The use of Sb as a surfactant during the growth of highly strained GaInAsN/GaAs QWs was also shown to achieve improved photoluminescence intensity and SQW laser diode characteristics[48].

Three-dimensional growth was observed for GaInAsN layers of thickness less than the critical thickness predicted by the Matthews and Blakeslee's model[36]. The reason may be due to N having a higher surface free energy than As and thus changing the surface growth kinetics. In contrast, Sb has a lower surface free energy than As, which favors wetting of the overlayer. However, the mechanisms of the island formation of GaInAsN and the role by which Sb affects the growth of GaInAsN are not fully understood.

In this thesis, the bandgap and band lineup of GaInAsN/GaAs are explained in chapter 2. Two different types of N plasma sources (ECR and RF) are used to grow GaInAsN (and GaAsN) by GS-MBE. The epitaxial layers of GaInAsN and GaAsN are characterized using double-crystal X-ray diffraction, PL at room and low temperatures, SIMS and Hall effect measurement. The growth techniques, characterization techniques,

and N incorporation behavior are described in chapters 3, 4 and 5, respectively. In order to improve the optical quality, post-growth and in-situ anneals were carried out on GaInAsN material. A comparison between as-grown samples and annealed samples is given in chapter 6 and an optimum anneal condition is determined. Transmission Electron Microscopy was also used to study the quantum well structures and the phase separation in a GaInAsN QW, which is attributed to the spinodal-like decomposition during the growth. The results are given in chapter 7 and a theoretical model of spinodal decomposition is described. In addition, SIMS and Hall effect measurements have been performed on GaInAsN of both as-grown and annealed samples, and these are discussed in relation to the PL properties in chapter 8. Finally, a conclusion and suggestions for future work are provided in chapter 9.

CHAPTER 2
Material properties of GaInAsN

2.1 Bandgap energy and lattice constant

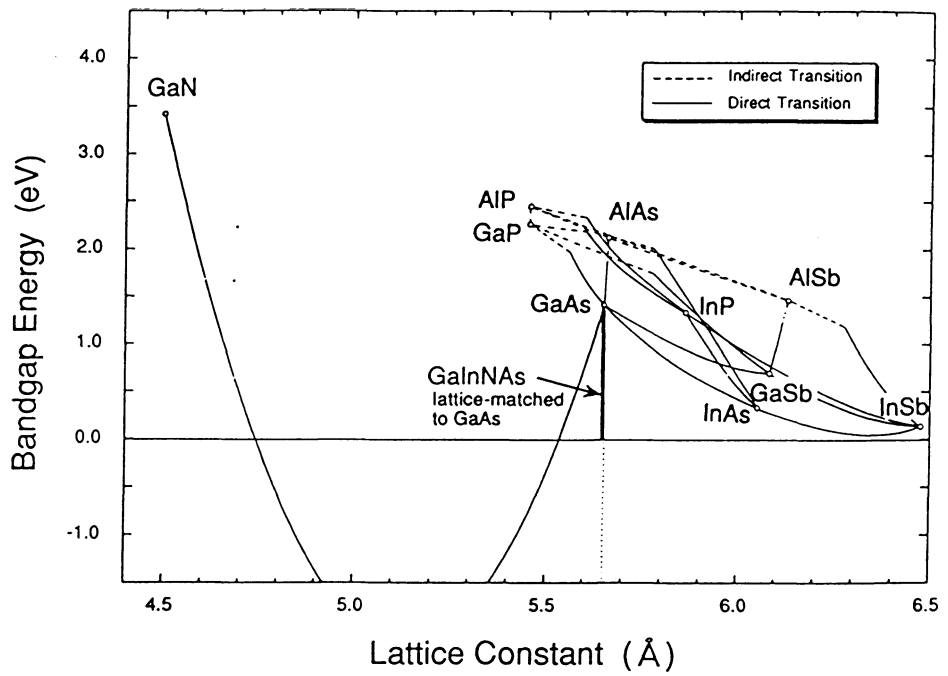

Fig.2.1 Relationship between E_g and lattice constant in III-V semiconductors (ref.9)

The relationship between the lattice constant and bandgap energy in III-V semiconductor alloys is depicted in figure 2.1. For the conventional III-V alloy semiconductors such as GaAsP, there is a general tendency towards increasing bandgap energy with decreasing lattice constant. However, for low nitrogen content GaAsN the bandgap energy decreases, instead of increasing, as would be expected. This curious phenomenon is explained in terms of the large discrepancy in electronegativity among the group V constitutuent atoms[23] (N: 3.00; As: 1.57; P:1.64). Also, nitrogen has the

smallest atomic radius among these atoms (N:0.072nm; As:0.123nm; P:0.113nm). So, incorporation of N into GaAs or GaInAs results in two effects; a decrease in lattice constant occurs due to the small size of the N atom, whilst the bandgap energy of the alloy is reduced due to the large electronegativity of N[23]. It is apparent in figure 2.1 that N incorporation can dramatically expand the range of accessible bandgaps in GaAs-based materials and result in a significant increase of freedom in the design of semiconductor devices. The fact that a region of negative bandgap energy also exists, as shown in figure 2.1, means GaAsN can behave as a metal or semi-metal or semiconductor depending on the N content.

Adding In to GaAs increases the lattice constant compared to GaAs, and adding N into GaInAs decreases lattice constant. Therefore, it is possible to grow GaInAsN lattice matched to GaAs by adjusting the relative content of In and N. Since GaInAsN is a direct transition semiconductor, it is a light-emitting material suitable for the production of long wavelength laser diodes on a GaAs substrate.

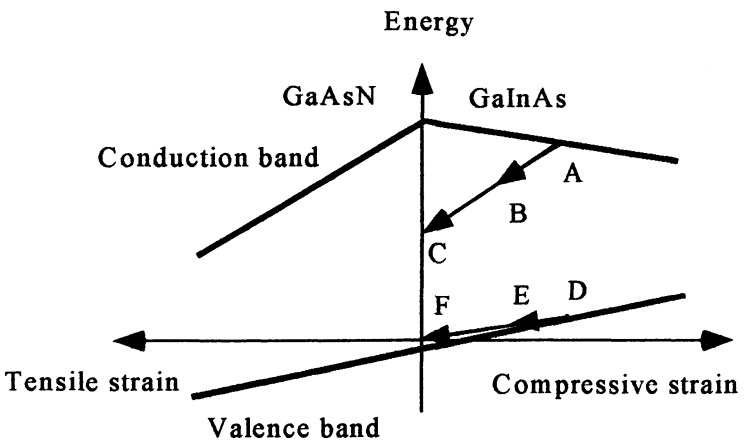

Fig2.2 Schematic diagram of the band lineup of GaAsN, GaInAs(N) (ref.9)

2.2 Band lineup of GaInAsN/GaAs

In order to produce an efficient semiconductor quantum well laser diode, a type-I band lineup between the well and adjacent barriers is necessary to confine both electrons and holes in the conduction band and valence band, respectively. The schematic diagram of the band lineup of GaInAs and GaAsN is shown in figure 2.2[9], and the band lineup of GaInAsN can be deduced. Increasing the content of In in GaInAs not only increases compressive strain, but also lowers the conduction band and raises the valence band, so the bandgap decreases with increasing In content. In contrast, increasing the content of N in GaAsN induces increased tensile strain and lowers both the conduction and valence bands, with the conduction band falling faster than the valence band. Thus, the bandgap is also decreased by adding N. In figure 2.2, Points A and D stand for the bottom of conduction band and the top of valence band of GaInAs material. As some N incorporate into GaInAs, the top of conduction band and the bottom of valence band move to points B and C, respectively. Points C and F correspond respectively to the bottom of the conduction band and top of the valence band for GaInAsN lattice matched to GaAs. It should be noted that the top of valence band of GaInAsN (point F) and GaAs differ only slightly, but this difference increases with the In content. Thus, hole confinement would be very small or non-existent resulting in an inefficient laser. Thus, by suitably combining compressively strained GaInAsN and GaAs, a type-I band lineup is achieved and the composition should be chosen such that a valence band discontinuity of at least 50meV should be achieved in order to produce sufficient hole confinement. Also, as can be seen in figure 2.2, the major part of the bandgap difference between GaAs and InGaAsN appears as the conduction band offset. This should allow the development of long wavelength lasers, e.g. operating at 1.3μm, with better temperature stability than

those produced with InGaAsP where the conduction band offset is about 40% of the bandgap difference.

The conduction band offset, ΔE_c, of GaInAsN plotted as a function of strain for the GaInAsN/GaAs system is shown in figure 2.3[64]. The addition of In to GaAs increases the compressive strain, while the addition of N into GaAs increase the tensile strain. Both In and N increase the conduction band offset $\Delta E_{c1}+\Delta E_{c2}$. This reduces

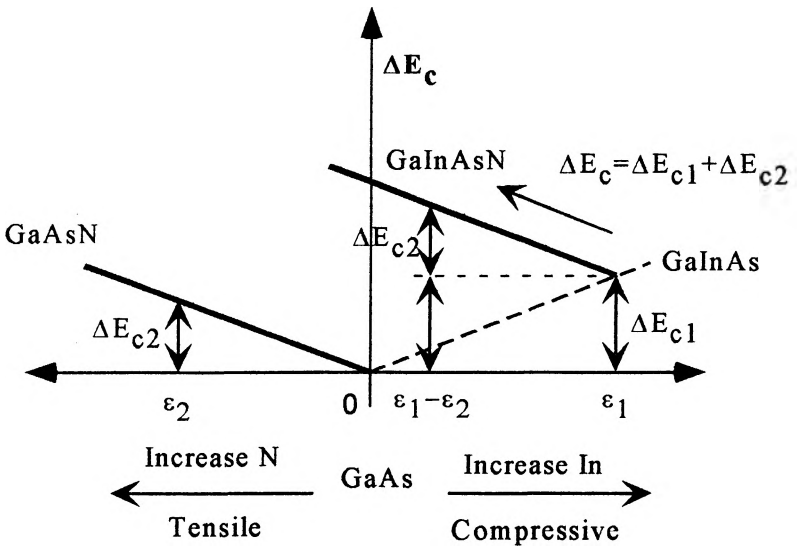

Fig.2.3 Schematic diagram of the conduction band offset as a function of the strain for GaInAsN/GaAs heterostructures (ref. 64)

electrons escaping from the GaInAsN well to the GaAs barrier layer compared to InGaAsP/InP lasers operating at the same wavelength, indicating that a GaInAsN

quantum well structure promises better high-temperature characteristics compared to conventional InGaAsP/InP long wavelength laser diodes.

Precise control of the nitrogen composition of GaInAsN is important since a small amount of nitrogen greatly affects the material properties such as bandgap energy and lattice constant. There are several methods for determining the nitrogen composition in GaInAsN and GaAsN: (1) Secondary Ion Mass Spectroscopy (SIMS); (2) X-ray diffraction; (3) Photoluminescence (PL). If the sample is strained, both X-ray and PL measurement are required if SIMS is not available. The quality of a GaInAsN QW can be evaluated from the PL intensity and linewidth of PL.

Using the low N content bandgap shrinkage coefficient of 150meV/(%N) for GaInAsN[24], a relationship between bandgap energy, E_g, and lattice constant, $\Delta a/a$, as a function of the In and N content for GaInAsN on GaAs has been calculated . This is shown in figure 2.4. The compositional-dependence data of E_g for InGaAs is obtained from reference 57. On the right side of figure 2.4, the bandgap at which 1.3μm of PL emission occurs is indicated. Thus, emission of this wavelength can be achieved by adjusting the relative In and N contents. However, the thickness of the $Ga_{1-x}In_xAs_{1-y}N_y$ layer is limited by the critical thickness[36], above which strain relaxation by dislocations occurs. Some critical thickness values are indicated on the bottom of figure 2.4, depending on the strain value.

For a GaInAsN QW, the PL peak position is not the same as the results shown in figure 2.4. The quantum size effect and strain effect will affect the electron-hole transition energy[58]. Again, assuming the same bandgap shrinkage coefficient of 150meV/(%N), and considering both the quantum size effect, for a 70 Å quantum well, and the strain effect, wells of different composition were designed to produce a PL

emission peak at ~1.3μm. Some results are shown in table 2.1. Consideration of the fact that the PL intensity is drastically reduced with increasing N concentration, only low N contents of 1-2% can be used. As can be seen from figure 2.4, reducing the N concentration has to be compensated by increasing the In content in order to maintain the emission at 1.3μm. However, increasing the In concentration leads to more compressive strain, which reduces the critical thickness. So the In content, N content and the QW thickness, have to be carefully controlled in order to produce a quantum well structure with the required emission wavelength. Some calculated results for the $Ga_{1-x}In_xAs_{1-y}N_y$ QW are shown in table 2.1.

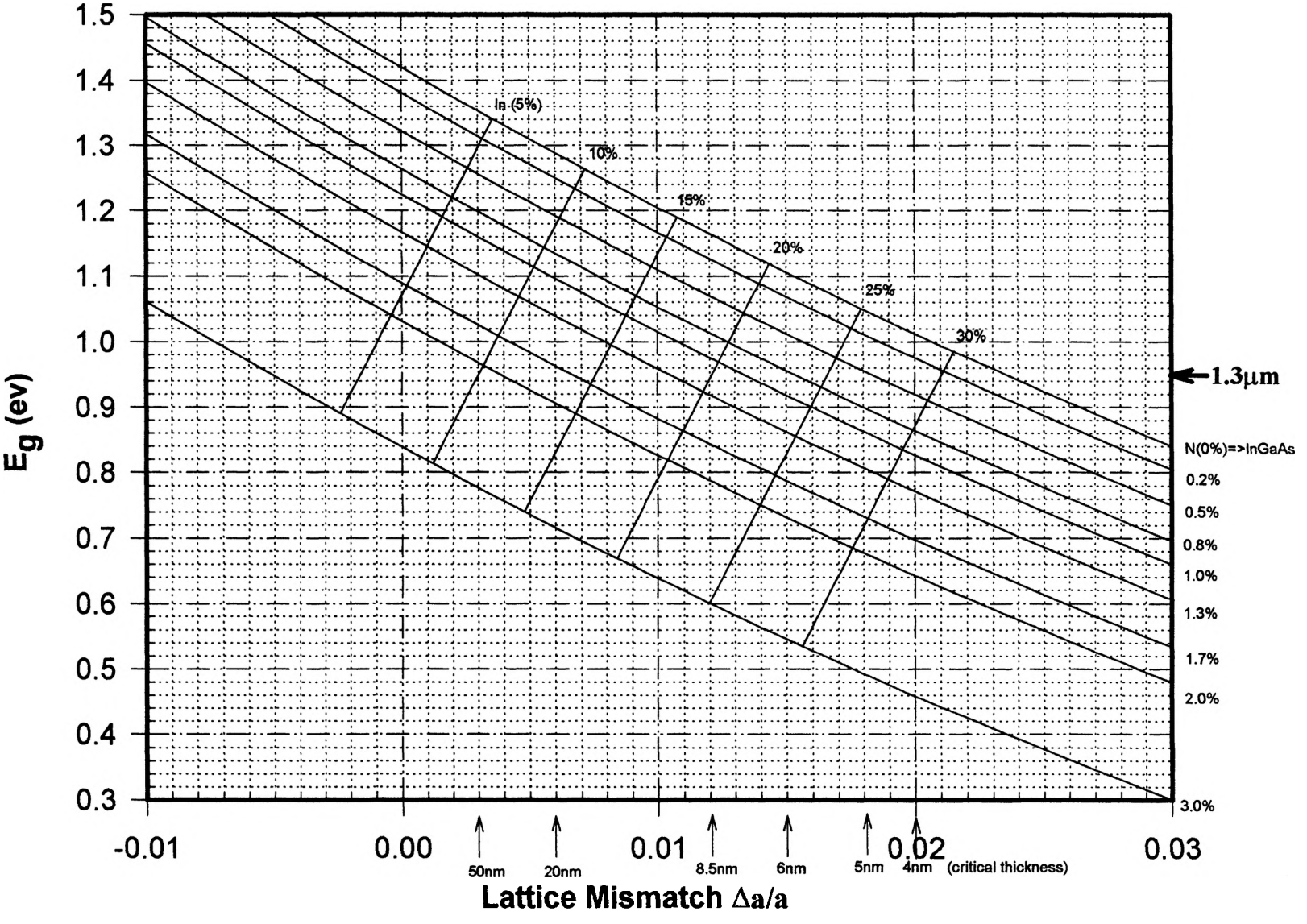

Fig.2.4 Calculated Eg versus Δa/a of bulk Ga1-xInxAs1-yNy/GaAs system

$In_xGa_{1-x}As$ QW(70Å)	Strain (Δa/a)	PL peak position (μm)	Adding N (%) into InGaAs	PL peak of GaInAsN (μm)	Strain of GaInAsN (Δa/a)	Critical thickness (Å)
$In_{0.18}Ga_{0.82}As$	0.013	0.976	2.1%	1.300	0.009	120Å
$In_{0.24}Ga_{0.76}As$	0.017	1.019	1.8%	1.310	0.014	70Å
$In_{0.26}Ga_{0.74}As$	0.019	1.034	1.7%	1.313	0.015	60Å
$In_{0.28}Ga_{0.72}As$	0.020	1.050	1.5%	1.297	0.017	50Å
$In_{0.30}Ga_{0.70}As$	0.021	1.066	1.4%	1.301	0.019	45Å
$In_{0.32}Ga_{0.68}As$	0.023	1.083	1.3%	1.305	0.020	40Å

Table 2.1 Calculated results of 1.3μm emission of GaInAsN QW (70Å)
(With the consideration of quantum size effect and strain effect)

CHAPTER 3
GS-MBE growth techniques

In the work of this thesis, GaInAsN and GaAsN materials were grown by gas-source molecular beam epitaxy (GS-MBE). The active N is produced by nitrogen plasma from either an RF plasma source or an ECR source. In this chapter, the GS-MBE technique is reviewed and the nitrogen plasma sources are briefly described.

3.1 GS-MBE system

Molecular beam epitaxy is a growth technique by which epitaxial layers are grown under ultrahigh vacuum conditions by impinging a thermal flux of atoms or molecules of the compositional species on the heated surface of a single crystal substrate. The temperature of the substrate must be high enough that the adsorbed atoms or molecules have sufficient mobility on the surface to move until they incorporate into appropriate, minimum energy, growth sites, but not too high that they have a high probability of evaporating before they become incorporated. The background partial pressure must be sufficiently low to meet the molecular flow conditions. This requires that the mean free path of the particles (atoms or molecules) in the beam is larger than the distance between the source and substrate.

Generally, the growth rate obtained in molecular beam epitaxy is low, ~1μm/hour (or about 1 monolayer/sec). This allows abrupt compositional or dopant changes to be made (normally within atomic dimensions) by shuttering the beam on a time scale of

<1sec.The growth temperature is typically ~550-630 ^{0}C for GaAs-based materials, so interfaces between layers of different composition remain abrupt since interdiffusion can be considered negligible. Another advantage of the MBE growth technique is the UHV environment which allows the whole range of surface analytical probes to be employed. These can be used to monitor both the chemical and structural properties of the crystal surface before, during, and after growth.

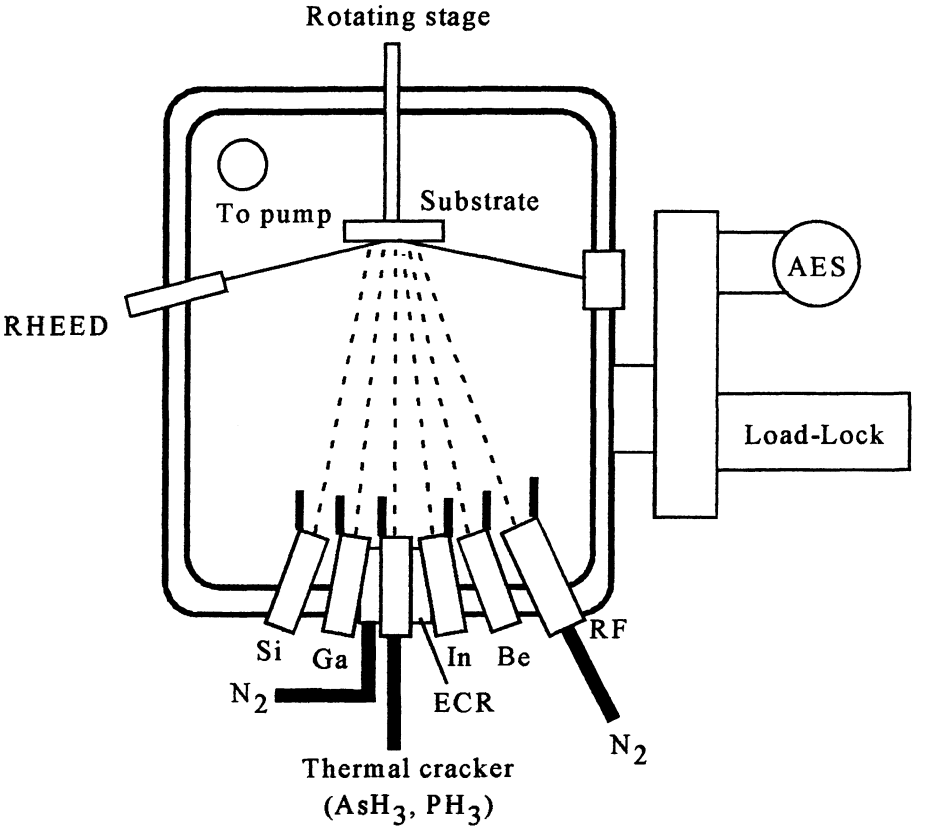

Fig.3.1 Schematic diagram of the GS-MBE growth system

Gas source MBE uses gaseous AsH_3 and PH_3 as group V sources with metallic Ga and In for the group III sources. For the group V species, the flux is controlled by a UHV

flow valve while the group III flux is controlled by the vapour pressure through the source temperature. Rapid changes in the dimer or monomer flux can be facilitated, so it becomes easy to control the layer composition.

The schematic diagram of our gas source molecular beam epitaxy system is shown in figure 3.1. The high vacuum in the MBE growth chamber is about 10^{-10} Torr. It is pumped by a liquid nitrogen trapped oil diffusion pump. Cryopanels filled with liquid nitrogen are used inside the MBE chamber to condense out water vapor, residual AsH_3 and PH_3, and other volatile contaminants.

The substrate temperature is usually controlled by a thermocouple that is 2mm behind the substrate. Absolute temperature measurement is carried out using infrared optical pyrometry. The pyrometry is calibrated at 525 ^{0}C where the surface reconstruction changes from 2x1 to 2x4, which is determined by reflective high energy electron diffraction.

Group III elements (In and Ga) and dopant elements (Si, Be) are evaporated from effusion cells. The requirement of the cells is that they provide stable fluxes of ultrahigh-purity beams which are uniform and appropriate intensity. The typical evaporation cells are inert containers, usually made of pyrolytic boron nitride (PBN). The advantage of this material is that PBN can be obtained with very low impurity levels (<10ppm) and dissociation of PBN doesn't occur until 1400 ^{0}C. Elemental In or Ga is placed within the effusion cell. Resistance heaters are used to heat the cells in order to achieve the required atom flux. Shutters are placed in front of each effusion cell to permit turning the effusion beam on or off. By precise temperature control of the effusion cells, the required group III composition (Ga/In ratio) is achieved.

With a gas source MBE system, the AsH_3 and PH_3 are decomposed in a single, low pressure cracker with a heated rhenium catalyst. The temperatures for efficient cracking of the hydrides to produce As- and P- dimers are typically 900-1000 ^{0}C. The major products of the dissociation are hydrogen, group III dimers, with some tetramers, and monomers. The relative amounts of the monomers, dimers and tetramers depends on the cell pressure and catalyst temperature. Usually more than 90% dimers are produced. The AsH_3 and PH_3 flows into the cracker cell are controlled using a baratron-based pressure control system and calibrated flow meters.

The substrates used in this thesis work are n-type or semi-insulting (100) GaAs prepared to be "epiready". This means no further processing is necessary before loading them into the growth chamber. The substrates are cleaved either in quarter pieces or in square pieces (15x15mm) from 400μm thick two-inch-diameter GaAs wafers. The n-type substrates are Si-doped with a carrier concentration ranging from 4-7x10^{18} cm^{-3}, and the semi-insulating substrates are EL2-doped with resistivities greater than 10^7 Ω-cm.

The substrate is loaded into the main growth chamber and heated to 580 ^{0}C. It is then exposed to an atomic-H flux for 5 min from an ECR source which is used to desorb surface oxides, whilst simultaneously exposing the substrate surface to an excess As_2 flux in order to protect the GaAs surface from dissociation.

After the cleaning stage, the group-V beam fluxes are adjusted to grow a layer of the required composition. Initially a buffer layer of the same composition as the substrate is deposited to cover any defects or impurities remaining on the substrate surface before growing the layer or structure of interest.

3.2 Nitrogen plasma sources

In order to grow III-V compounds containing nitrogen, a source of active nitrogen is required. Due to very large bonding energy of the nitrogen molecule (9.9 eV) in the ground state, nitrogen molecules do not thermally dissociate at normal MBE growth temperatures. Thus, plasma sources are used where sufficient energy can be transferred to the molecule to allow dissociation. Two kinds of plasma sources are used in this thesis work for producing active N species. One is an electron cyclotron resonance (ECR) source, the other is a radio frequency (RF) plasma source.

3.2.1 ECR plasma source

A Microscience ECR-900 series electron cyclotron resonance source was used, which employs an axial electromagnet to stimulate a resonant coupling of the microwave energy (with a frequency of 2.45GHz) with the electrons in the discharge zone.

The forward microwave power applied in the experiments was normally around 300W. The absorbed power is about 100W. The input nitrogen flow is between 0.1-1 sccm.

3.2.2 RF plasma source

The RF plasma source in our work is RF plasma source (EPI company provided). A schematic diagram is shown in figure 3.2. Both the discharge tube and beam exit plate are made of pyrolytic boron nitride, as all-PBN construction minimizes possible O contamination from the source. The RF coil around the discharge tube is water cooled.

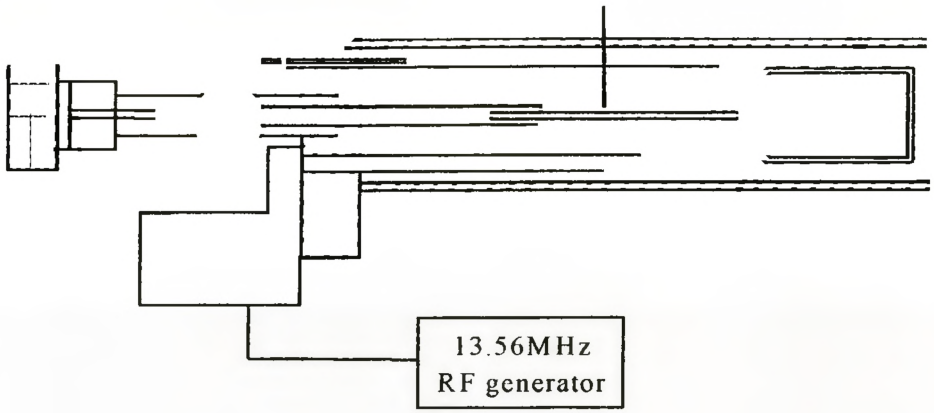

Fig.3.2 Schematic diagram of an RF plasma source

The RF source is excited with inductively coupled 13.56 MHz power supplied by an RF generator. The gas conductance into the MBE chamber can be changed using different outlet plates containing different numbers of holes. Plates with 25, 50, 66, and 253 holes were supplied. The diameter of all holes is 0.008 inch.

The RF power, flow of input nitrogen gas, and flow conductance at the exit of plasma discharge tube are parameters affecting active N production. The RF power used for our EPI RF plasma source ranges from 65W to 500W. At least 65W is required to strike a plasma. The input nitrogen flow rate used ranges from 0.1~ 1sccm. The relationship between RF power, N_2 flow rate and the amount of the active N produced is described in the next section.

3.2.3 OES characterization of plasma sources

Optical emission spectrometry (OES) is the spectral analysis of the light emanating from excited atoms and molecules. By measuring the wavelengths and intensities of the emitted spectral lines, one can identify the neutral particles and ions present in the plasma, because each atom, molecule and ion has its own characteristic emission lines. OES is most widely used for monitoring and diagnosis of plasma processes.

For the excited nitrogen of interest in this work, a number of emission peaks associated with neutral nitrogen molecules involving the 1st positive and 2nd positive series of molecular transitions[49,50] are observed. The strongest emission peaks of the 1st positive series of the molecular nitrogen series ($B^3\Pi_g \rightarrow A^3\Sigma_u^+$ transitions) occur at wavelengths of 540, 590, 660, 760, 820nm. The largest peaks of the 2nd positive molecular nitrogen series ($C^3\Pi_u \rightarrow B^3\Sigma_g$ transitions) occur at 316, 337, 357, 380, and 400nm. The most intense lines of the 1st negative series of N_2^+ molecular ion transitions ($B^2\Pi_u^+ \rightarrow X^2\Sigma_g^+$) are at 391 and 428nm. For atomic nitrogen, sharp atomic nitrogen emission lines occur at 745, 821, and 869nm. The "active" nitrogen responsible for III-V nitride thin film growth is most likely a mixture of 1st positive series nitrogen molecules and atomic nitrogen, while the 2nd positive series nitrogen molecules and nitrogen molecular ions doesn't appear to contribute substantially to the growth of nitrides[38]. The latter may even cause ion damage to the crystal due to their higher energy.

Optical emission spectra from our RF plasma source were measured. Unfortunately, because there is no observation port on our ECR plasma source, direct measurement of optical emission spectra in our ECR plasma source is not possible. W.C. Hughs[38] measured the optical emission spectra of an ECR source and compared it to

that of an RF source. The results are shown in figure 3.3. It is seen that the ECR nitrogen plasma contains a much higher N_2^+ ion density and 2nd positive molecular series nitrogen than an RF plasma. In our study of the EPI plasma source, the optical emission is predominantly from atomic N and the 1st molecular series and there are almost no characteristic peaks of N_2^+ ions (391 and 428nm) and of the 2nd positive molecular series at 316, 337, 357, 380, and 400nm. The optical emission spectrum from our source is shown in figure 3.4. It is seen that atomic N and 1st positive series molecular nitrogen dominates.

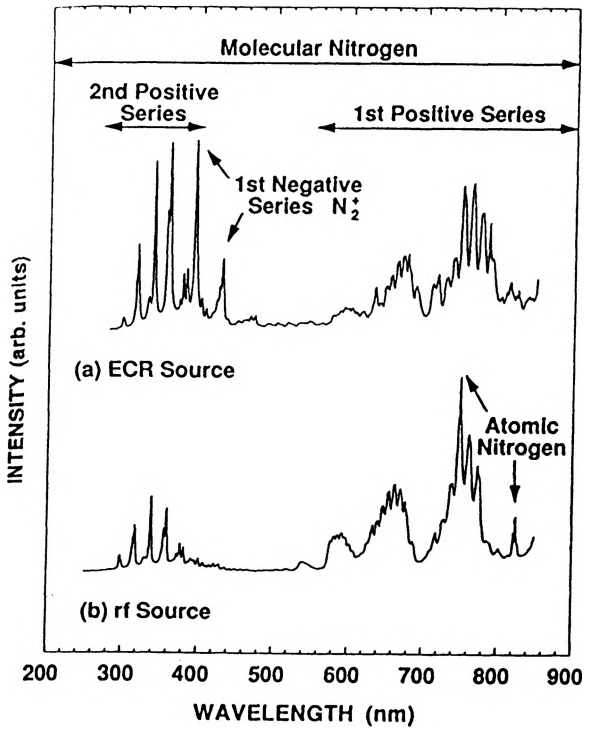

Fig.3.3 Comparison of optical emission spectra for ECR and RF plasma sources (from Ref.38)

Active N production is directly affected by three factors: (1) RF source power; (2) input N_2 gas flow; and (3) conductance of the output aperture of the RF source. To establish the optimum working conditions, it is important to carry out detailed characterization experiments.

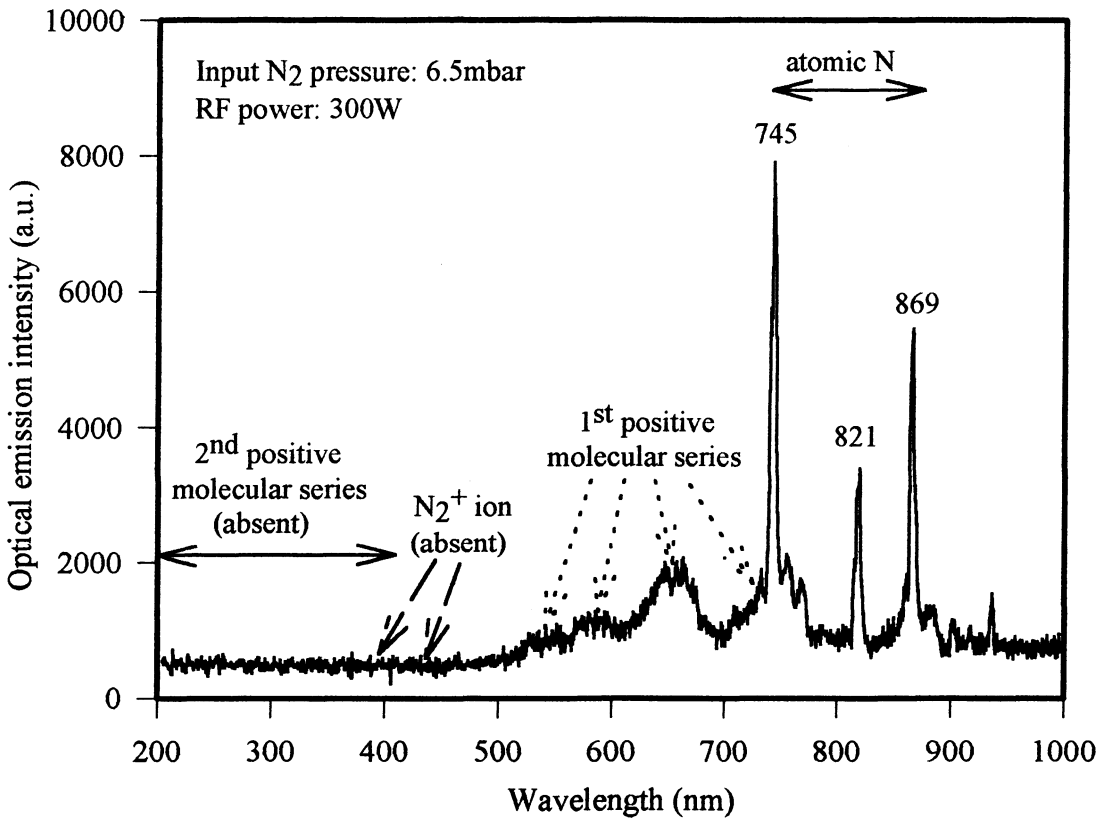

Fig.3.4 Optical emission spectra of EPI RF nitrogen plasma source

(1) RF source power. The working power range of the RF source is between 65W and 500W; at powers below 65W, a plasma can not be sustained. Figure 3.4 shows a typical optical emission spectrum of an RF plasma obtained for an RF power of 300W and a N_2 input pressure of 6.5mbar. The amount of the active nitrogen (both atomic N and 1st molecular series) can be increased by increasing the RF power. It was observed that for a constant N_2 input flow, increasing the RF power mainly increases the atomic N level.

(2) N_2 gas flow. Increasing the input nitrogen flow was found to mainly increase the 1st molecular series rather than atomic N. The reason might be the high nitrogen gas pressure in the source leads to high recombination of atomic N, so the relative density of the molecular series increases. There are two kinds of modes of the RF plasma, a bright mode and a dark mode. A high pressure of nitrogen gas will switch the plasma mode from the bright-mode to the dark-mode, which is not suitable for nitride growth. All our growths of the nitride materials in this thesis work were carried out using the bright-mode region.

(3) Conductance of the exit aperture. It has been reported in MBE growth of GaN that a high pressure in the RF cell is better for suppression of the ion generation rate[28]. Thus, a low exit conductance is required. In our experiments, we found that the use of a lower conductance exit aperture allowed us to grow nitride samples with higher N content. The lowest conductance of the exit apertures of RF plasma source in our experiments was ~90cm^3/sec. Detailed experiments comparing the quality of GaInAsN samples grown with different conductance apertures have not been carried out.

CHAPTER 4
Characterization techniques

Various experimental techniques were used to characterize the crystal quality and the optical quality of the GaInAsN epitaxial films grown in this work. These include double-crystal X-ray diffraction; room-temperature photoluminescence; low-temperature photoluminescence, transmission electron microscopy; Hall effect measurements; and SIMS measurements.

4.1 Double-crystal X-ray diffraction

Double crystal X-ray diffraction is a non-destructive method for analyzing the structural properties of thin crystalline layer. For a beam of X-rays incident at an angle θ on a set of plane with lattice spacing d, the diffracting beam will be constructively enhanced if they meet the well known Bragg condition: $2d\sin\theta=m\lambda$, where m is an integer, and λ is the X-rays wavelength. This can be used to obtain the lattice constant of the film; hence information on the composition.

The schematic diagram of the Bede Scientific Instruments QC1 double crystal X-ray diffractometer is shown in figure 4.1. The X-ray beam is incident on the first reference crystal which acts as a narrow band filter and a collimator. Only the beam with wavelength and incident angle satisfying the Bragg condition is then incident on the sample. This results in a high resolution spectrometer. The X-ray source emits Cu K_α radiation, i.e., Cu $K_{\alpha1}$(1.541Å) and Cu $K_{\alpha2}$(1.544Å). The reference crystal disperses the

$K_{\alpha 1}$ and $K_{\alpha 2}$ lines such that only one is incident on the sample crystal, selected by the Bragg condition.

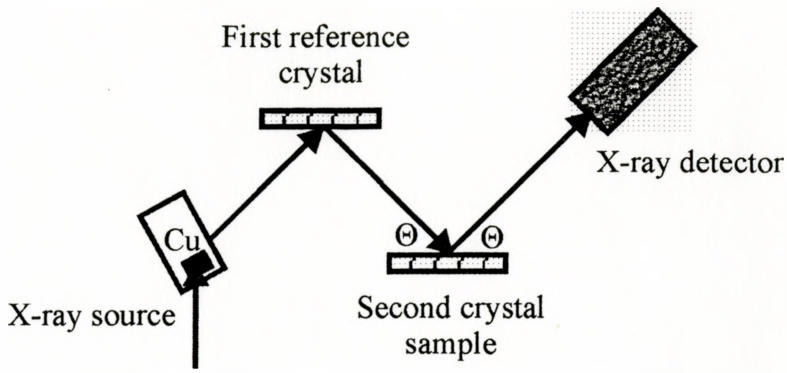

Fig.4.1 Schematic diagram of double-crystal X-ray diffractometer

The Bragg angle for GaAs (a=5.6533Å) is 33.04^0 for $K_{\alpha 1}$ (λ=1.541Å) radiation. Without separating the K_α lines the spectral linewidth will be broadened since it will be a combination of both lines.

As indicated in chapter 2, the addition of In and N to GaAs changes the lattice constant and hence introduces strain to layers deposited epitaxially on GaAs. When the thickness of the epitaxial layer is less than the critical thickness, predicted by Matthews and Blakeslee[36], the epitaxial layer is strained but coherent, which means the lattice spacing in the plane of growth is the same as that of the substrate. Neglecting the effects due to bending of the substrate by the strained epitaxial layer, all of the strain is taken up by a tetragonal distortion of the lattice unit cell of the layer. By differentiating Bragg's law, it is possible to relate the lattice mismatch of the unconstrained layer, ($\Delta a/a$), to the angular separation, $\Delta\theta$, of the layer and the substrate peaks obtained from the x-ray rocking curve as[51]:

$$(\Delta a/a) = -(\Delta\theta \cot\theta)(1+2C_{12}/C_{11})^{-1}$$

where θ is the Bragg angle of the substrate, and C_{11} and C_{12} are the elastic constants of the layer. For the ternary GaAsN and quaternary GaInAsN, the values of C_{11} and C_{12} are interpolated from those of the binary constituents using Vegard's law. The elastic constants, C_{11},C_{12}, C_{44}, for GaAs, GaN, InAs, InN, and their lattice constants are listed in table 4.1.

If the thin epitaxial layer has uniform thickness and a well-defined and flat substrate interface, multiple diffraction of the diffracted X-ray beam occurs from different atomic planes before leaving the sample. This leads to a number of weaker, equally spaced reflection peaks observed in addition to the main peaks of the substrate and the epitaxial layer. These weaker peaks are called "Pendellosung fringes". The thickness (d) of the epitaxial layer can be deduced from the angular separation of Pendellosung fringes ($\delta\theta$) through:

$$d = \lambda/2\, \delta\theta \cos\theta$$

4.2 Room-temperature and low-temperature photoluminescence

Photoluminescence is one of the most powerful optical techniques for studying and characterizing semiconductor materials. It is non-destructive, sensitive, and is typically used to determine the semiconductor bandgap. It can also yield information on impurities and defects, which may affect material quality and device performance.

When a semiconductor is optically excited by a laser with photon energy greater than the bandgap energy, electron-hole pairs are generated. These electron-hole pairs

relax to the lowest available energy level, usually the bottom of the conduction band for the electron and the top of the valence band for the holes before recombination. Because of the direct nature of the bandgap in GaAs and related compounds, the recombination proceeds through emission of photons with energies equivalent to the bandgap energy.

Table 4.1 Material parameters of GaAs, GaN, GaP, InAs, InN, InP

	GaAs	GaP	GaN	InAs	InP	InN
Lattice Constant a (Å)	5.6533	5.4512	4.52[2]	6.0584	5.8688	4.98[2]
Elastic constant $C_{11}(10^{10}Pa)$	11.88	14.12	28.2[3]	8.33	10.22	18.2[3]
Elastic constant $C_{12}(10^{10}Pa)$	5.38	6.25	15.9[3]	4.53	5.76	12.5[3]
Elastic constant $C_{44}(10^{10}Pa)$	5.94	7.05	14.2[3]	3.96	4.60	7.9[3]
Poisson ratio ν	0.312	0.307	0.361	0.352	0.360	0.407
Shear modulus μ $(10^{10}Pa)$	3.25	3.925	6.15	1.90	2.23	2.85
Young's modulus E $(10^{10}Pa)$	8.53	10.28	16.74	5.14	6.07	8.02

Reference: (1): Sadao Adachi, J. Appl. Phys., **53**, 8775, 1982

(2): T. Azuhata, J. Phys.: Condens. Matter., **8**, 3111, 1996

(3): Kwiseon Kim, Phys. Rev. B, **56**, 7018, 1997

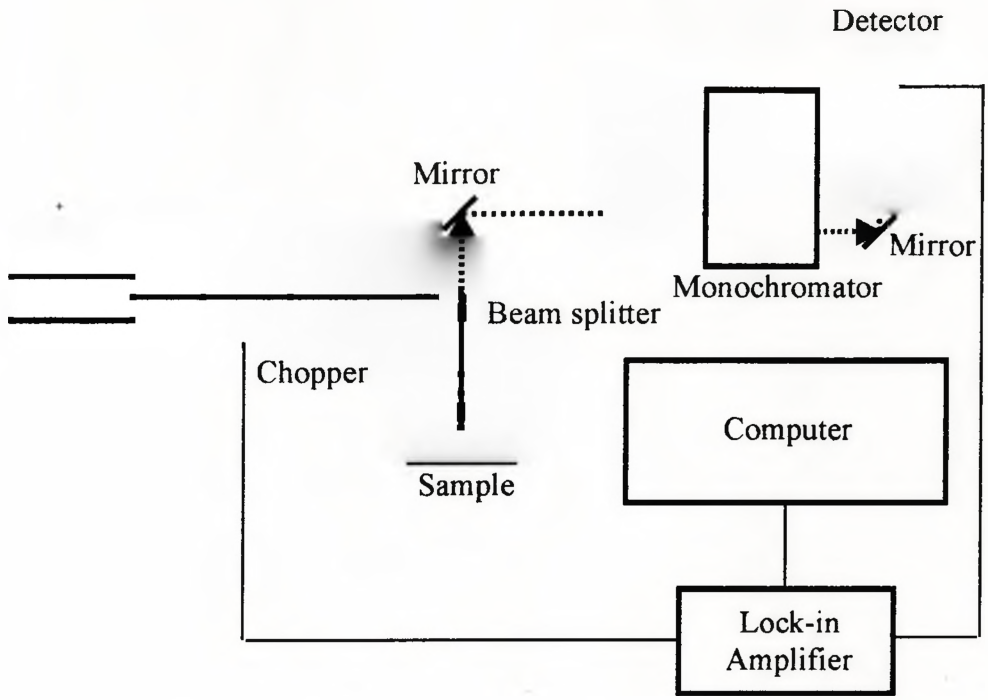

Fig.4.2 Schematic diagram of RT-PL measurement equipment

There are many possible radiative recombination mechanisms: (1) band-to-band recombination; (2) free exciton transition; (3) excitons bound to a donor or acceptor transition; (4) donor-acceptor pair transitions; and (5) conduction band to acceptor transitions. Recombination at room temperature is primarily via band-to-band transitions yielding a measurement of the bandgap. At low temperature, the transitions are mainly excitonic in nature giving a value of the bandgap less some small exciton binding energy. Thus PL is mainly used to determine the bandgap energy. Recombination via an intermediary state (i.e. deep state) is primarily non-radiative in nature. Auger recombination is another nonradiative recombination process involving a three body interaction which can have many forms. Most of the recombination mechanisms give rise

to broad emission lines, while the excitonic recombination usually gives narrow emission lines.

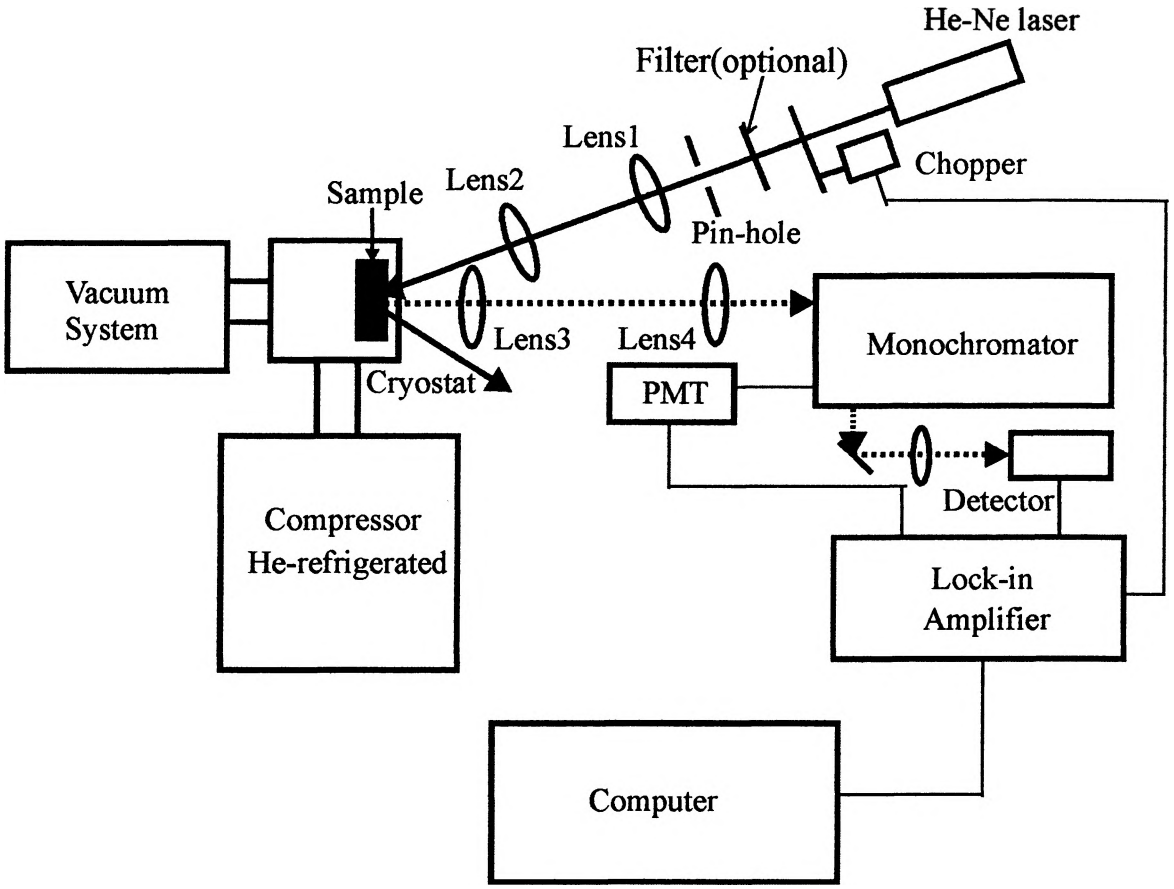

Fig.4.3 Schematic diagram of LT-PL measurement equipment

The schematic diagram of the room temperature photoluminescence measurement equipment is shown in figure 4.2. The pump source is a CW Ar^+ laser, which emits at 514.5nm and 488nm. The filter is used to block the 514.5nm lasing line so the excitation is due only to the 488nm line. A Lock-in amplifier technique is used to increase the

detection sensitivity. After passing through a monochromator, the photoluminescence signal intensity is measured using an InGaAs detector. In order to compare the PL intensity of many samples prepared with different growth conditions or different annealing conditions, and over the long period of time necessary to carry out this research, a reference sample is used to compensate for any changes in the output intensity of Ar^+ laser over time.

A schematic diagram of the low-temperature photoluminescence measurement system is shown in figure 4.3. The pump source is a 10mW He-Ne laser with a wavelength at 632.8nm. Similar detection electronics to RT-PL set-up are used. Lens 1 and lens 2 are used to focus the laser beam onto the surface of the sample, and lens 3 and lens 4 to collect the photoluminescence into the monochromator. A 600 lines/mm grating is used in the monochromator for the PL wavelength from 0.8μm to 1.8μm. Another, 1200 lines/mm grating is available for wavelengths from 0.4μm to 1.1μm, which was not used in our experiments. An InGaAs pin photodetector is used for the wavelengths from 0.9μm to 1.65μm. The base temperature of the sample is 15K obtained using a closed-cycle, helium-refrigerator. Various temperatures between 15K and room temperature are obtained using a resistive heater. The temperature is measured by a calibrated thermocouple mounted on the cold-head below the sample. By setting the size of the entrance and exit slits of the monochromator at 0.5mm, a resolution of 1nm is achieved. The monochromator is calibrated using the He-Ne laser line (632.8nm) to ensure the wavelength accuracy.

The advantage of making the photoluminescence measurements at low temperature is that thermally-activated, non-radiative recombination processes and thermal broadening of the spectral line can be reduced. As the temperature decreases, the

position of the band-band transition is shifted to shorter wavelengths as the bandgap energy increases according to the Varshni equation[52]:

$$E_{g(T)} = E_{g(T=0)} - \alpha T^2/(T + \beta)$$

where $E_{g(T)}$ is the bandgap energy at a certain temperature (Kelvin), and $E_{g(T=0)}$ is the bandgap energy at zero Kelvin, α and β are material dependent parameters.

4.3 Transmission Electron Microscopy

Cross-sectional transmission electron microscopy (TEM) was used for the study of the compositional modulation of GaInAsN epitaxial quantum wells grown for this study. A Philips CM12 microscope operating at 120kV was used. Sample preparation for the TEM analysis was as follows: (1) two strips (about 7x1mm^2) are cut from the wafer and glued with epitaxial sides face-to-face to form the central part of the cross sectional TEM sample, 4 silicon strips of the same size are glued to both sides of the GaInAsN sample; (2) the glued sample is mechanically polished to a thickness about 300 μm; (3) a 3mm diameter disc is cut from the raft using an ultrasonic disc cutter, then mechanically polished again down to 100μm; (4) both sides of the disc are then dimpled using a dimpler until the central thickness of the disc is about 30 μm; (5) finally, the thinned disc is ion milled using an Ar ion beam for about 15 hrs to 20hrs.

Under the two beam condition, both bright field and dark field cross sectional TEM micrographs were obtained using diffraction vectors **g**=022 and **g**=400. The diffraction vector **g**=022 is sensitive to the compositional modulation along the [0 –1 1] direction[65]. In order to observe the compositional modulation caused by the N

incorporation into InGaAs, several samples with and without N were grown. Detailed results of the TEM analysis are provided in chapter 7.

4.4 Hall effect measurements

In order to demonstrate the existence of carrier traps in the expitial GaInAsN material and obtain a rough estimate of the concentration of these traps, room-temperature Hall effect measurements were done on un-doped, n-type (Si-doped - $4x10^{17}/cm^3$), p-type (Be-doped -$4x10^{17}/cm^3$) $Ga_{0.955}In_{0.045}As_{0.985}N_{0.015}$. Samples were also measured after thermal annealing at 725 ^{0}C for 30min.

The samples were configured in a $5x5mm^2$ square, Van der Pauw geometry[54]. Small area metal contacts were formed at the four corners of the samples to obtain ohmic contacts. A schematic diagram of the Hall sample is given in figure 4.4. For n-type material, Sn is used as the contact metal; and for p-type material, In:Zn (95:5) is used. Small spheres of the contact metal are placed at the four corners and the ohmic contact is formed by heating it to ~200 ^{0}C in an environment of flowing $HCl:N_2$. The flowing $HCl:N_2$ atmosphere removes the surface oxide, allowing a good ohmic contact to be formed. To ensure the ohmic nature of the contacts the resistance from contact-contact is measured using an ohm-meter. For good ohmic contacts all four contact-contact measurements should have similar resistance and be independent of the polarity of the probes.

The resistivity measurement of the sample is done by measuring the applied current and voltage drop in the absence of a magnetic field. Current is applied to two adjacent contacts and the voltage measured across the other two contacts. For example,

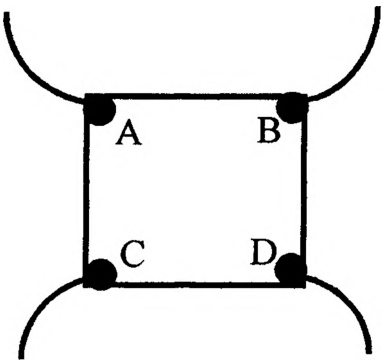

Fig.4.4 Schematic diagram of Hall effect measurement sample

$R_{AB,CD}$ means the resistance measured across C and D when the current is applied through A and B, $R_{AB,CD}=V_{CD}/I_{AB}$. $R_{BA,CD}$ means the resistance measured across C and D when the current applied through A and B is reversed. With the assumption of uniformity of both thin film thickness (d) and the transport properties within the thin film layer, the resistivity (ρ) is given by the formula:

$$\rho = \frac{\pi d}{\ln 2}\left\{\frac{\left|R_{AB,CD}\right| + \left|R_{BA,CD}\right| + \left|R_{BD,AC}\right| + \left|R_{DB,AC}\right|}{2}\right\} f\left\{\frac{R_{AB,CD}}{R_{BC,DA}}\right\}$$

where $f\{R_{AB,CD}/R_{BC,DA}\}$ approximates unity for a square sample.

The mobility and carrier concentration measurements are carried out when the magentic field B is present. The magnetic field is applied normal to the sample surface, in either direction +B or reverse direction -B. Now the current is applied across the sample diagonally (e.g. I_{AD}, or I_{BC}) and the voltage is measured across the other two contacts (V_{BC} or V_{AD}). The measurements are repeated with the current reversed. The same set of

measurement is repeated with the magnetic field reversed. The Hall coefficient R_H is obtained from the expression:

$$R_{H(n,p)} = \frac{R_{H(AD,BC)} + R_{H(DA,BC)} + R_{H(BC,AD)} + R_{H(BC,DA)}}{4}$$

where $R_{H(AD,BC)}$ is:

$$R_{H(AD,BC)} = \frac{d}{2B}\left(\frac{V_{BC}(+B)}{I_{AD}(+B)} - \frac{V_{BC}(-B)}{I_{AD}(-B)}\right)$$

The carrier concentration (n,p) is determined by[55]:

$$n, p = \frac{r_H}{eR_{H(n,p)}}$$

where r_H is the Hall scattering factor, assumed to be isotropic and unity. The mobility (μ_n,μ_p) can be obtained from the equation:

$$\mu_n, \mu_p = \frac{R_{H(n,p)}}{\rho}$$

The magnetic field B used in our experiment was fixed at 0.2 Tesla.

The main source of error in these measurements is the presence of a depletion layer at the surface of the sample and at the interface between the epitaxial layer and the substrate. This means that the "conducting" thickness of the layer is less than its physical thickness. The "conducting" thickness is needed in order to obtain the resistivity and carrier concentration. We have used the measured depletion layer thickness versus carrier concentration for GaAs[66]. At low carrier concentrations the results become unreliable since the 2μm thick epitaxial layer becomes fully depleted. The second error source is the

quality of the contact. This can be minimized by measuring the resistance between contacts as mentioned above and ensuring that the contact-contact resistance is uniform and not too high. One additional problem was a drift of ~5% in the magnetic field over the measurement time.

4.5 SIMS

Secondary ion mass spectrometry (SIMS) is a sensitive analytical technique that can reveal compositional information for dopants, impurities and compositional components present at low concentration (≤ a few %). This method has high elemental resolution and excellent depth resolution (<50Å)[53]. The structures analyzed can be thick bulk materials or layered structures.

For SIMS analysis, the sample is bombarded with a focused energetic beam of ion (typically Ar^+, O^+ or Cs^-) with energies in the range of 0.5 to 20keV. This sputters atoms from the topmost surface of the sample which are emitted as ions and atoms. Although the amount of secondary ions is only a small fraction (from 10^{-4} to 10^{-1}) of the sputtered atoms the detection system is very sensitive. The sputtered ions (positive or negative) are collected through an energy filter and mass analyzed yielding the composition of the topmost layer of the sample. If the sputter rate is in the dynamic SIMS range, the surface of the sample is continuously eroded during the analysis time. Thus the concentration of all sputtered atom species can be determined as a function of time which can subsequently be converted into depth information.

SIMS is used in this work to determine the N and In contents in the GaInAsN epitaxial sample. This is used as verification of the composition value determined from

X-ray diffraction and room-temperature photoluminescence. Since we observed that the PL intensity from a GaInAsN QW is much weaker than from a GaInAs QW with the same In content, SIMS was used to determine whether impurities such as O, H, C, Si, B were present in the QW. In order to compare the composition and any impurity concentration variation of the samples before annealing and after annealing, two sample pieces from the same growth sample were analyzed by SIMS, one was as-grown and the other had been annealed at 700 ^{0}C for 1.5 hours. These SIMS measurements were carried out by Dr. Richard W Streater, Advanced Technology Group, Nortel Networks, Ottawa. Details of the sample structure used for the SIMS measurements are provided in chapter 8.

CHAPTER 5
Nitrogen incorporation in GaAsN and GaInAsN

5.1 Active nitrogen production

Three methods are typically used to produce active nitrogen in the molecular beam epitaxy system. The first approach uses thermal decomposition of ammonia as a nitrogen source; the second method uses plasma-activated molecular nitrogen; and the third way utilizes low-energy ionic, N_2^+, nitrogen. However, the last method was only reported in GaN growth[59]; no previous GaInAsN growth using this method has been reported.

In our initial experiments of Ga(In)AsN growth, ammonia was either thermally cracked (700 ^{0}C-900 ^{0}C) or ECR plasma activated to produce a source of active nitrogen. A small amount of nitrogen incorporation in both GaAsN and GaInAsN was achieved, however, the nitrogen incorporation is not consistent for continuous growths. This problem may result from the high reactivity of ammonia with various filaments heating the effusion cells, substrate and ionization gauges.

Active nitrogen was successfully produced by a nitrogen plasma source. An RF plasma source provides better performance than the ECR plasma source because the RF plasma source produces less energetic N_2^+ and 2nd molecular nitrogen series than the ECR source. These species are thought to cause ion damage in the material [24, 38].

The production of nitrogen plasma is directly related to both the RF power and the input, N_2, gas flow. Optical emission spectra were taken for nitrogen RF plasma with an aperture configuration consisting of 25 holes of 200 μm diameter. Figure 5.1 shows the measured optical emission spectra of N_2 plasma. The main products of the

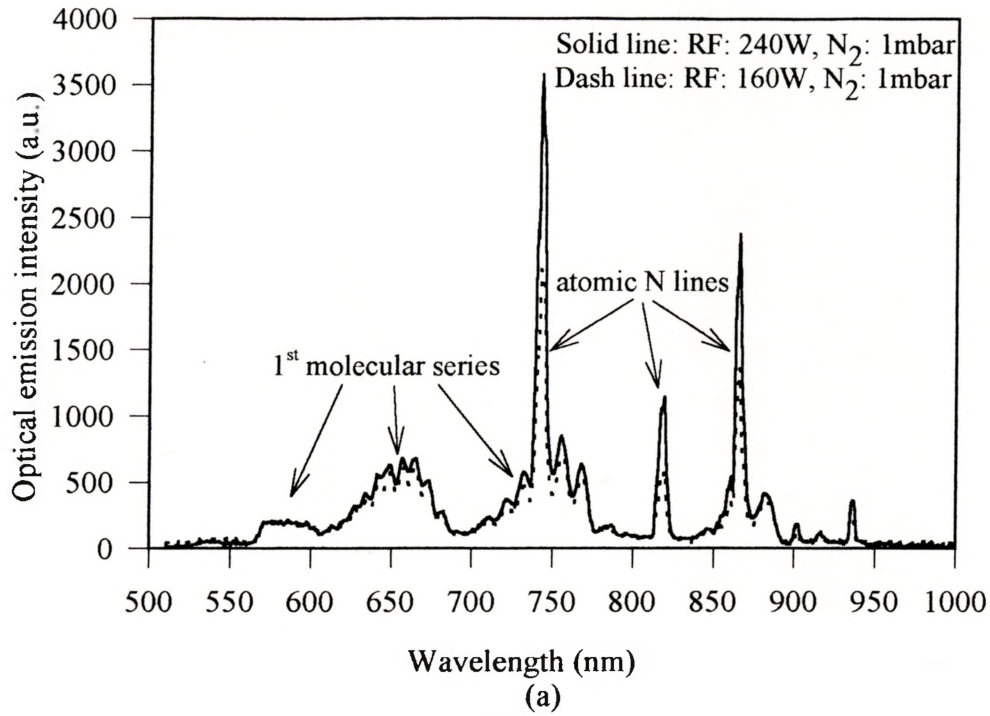

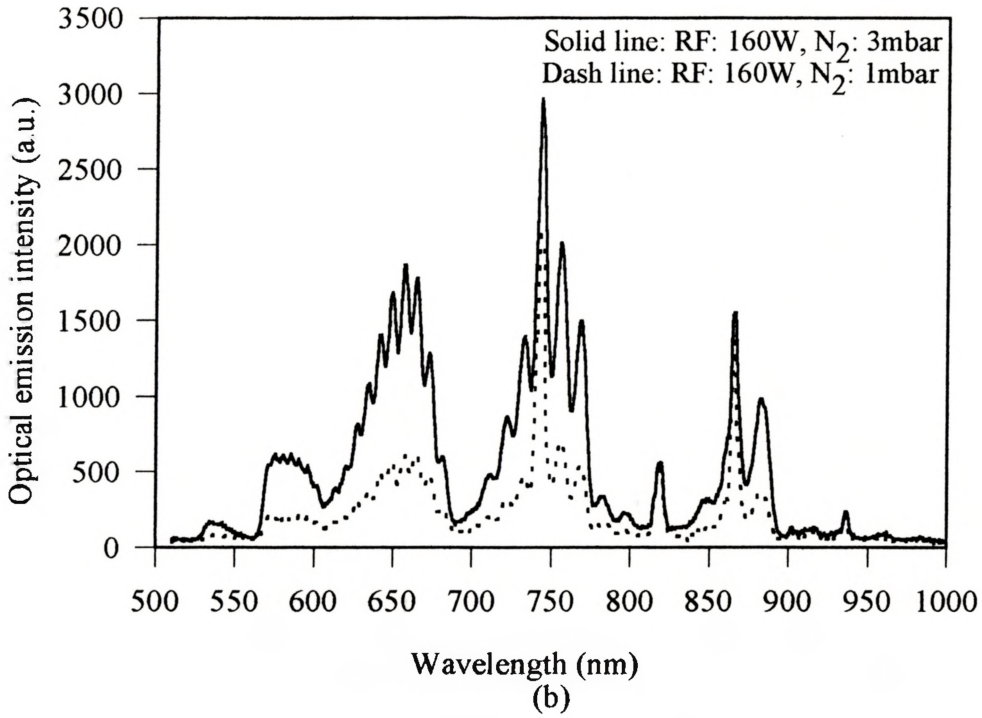

Fig.5.1 Optical emission spectra of a RF nitrogen plasma, (a) comparsion between different power with N_2 flow fixed; (b) comparision between different N_2 flow with RF power fixed

nitrogen plasma consist of atomic N and the 1st molecular series. Figure 5.1(a) displays the optical emission variation due to the changing of RF power with a fixed nitrogen flow, while figure 5.1(b) shows the optical emission variation due to the change of input nitrogen flow at a fixed RF power. It can be concluded from figure 5.1 that increasing both RF power and nitrogen flow can increase the active N content in the plasma. However, in order to obtain more atomic N rather than the 1st molecular series, it is necessary to increase the RF power but keep a low input nitrogen flow as shown in figure 5.1(a). Increasing the nitrogen flow mainly contributes to the enhancement of the 1st molecular series as shown in figure 5.1(b).

5.2 Factors affecting N incorporation in GaAsN and GaInAsN

Four samples (#2864, #2911, #2906, #2920) were grown at a temperature of 515 ^{0}C to study the relationship between N concentration in GaAsN and applied RF power. The RF source conductance was defined by the 25x200μm exit aperture. A 1000 Å thick GaAs buffer layer was grown first on the (100) GaAs substrate. Then a GaAsN layer was grown using the RF plasma nitrogen source. The concentration of incorporated nitrogen was determined by X-ray diffraction and calculated from the peak angle, and the difference between the strained layer and GaAs substrate peaks. Incorporation of 1%N corresponds to an angular difference, $\Delta\theta$ of 520 arcseconds. This value was calculated from the lattice constant and elastic constants shown in table 4.1. In order to make photoluminescence measurements on the GaAsN samples, 250 Å InGaP layers grown lattice matched to GaAs were deposited on both sides of the GaAsN epitaxial layer. A 200 Å GaAs cap layer was also grown to protect the sample surface and prevent As loss during anneals. These additional layers, the GaAs anneal cap and the InGaP barriers, should not affect the X-ray determination of the N concentration because they are lattice

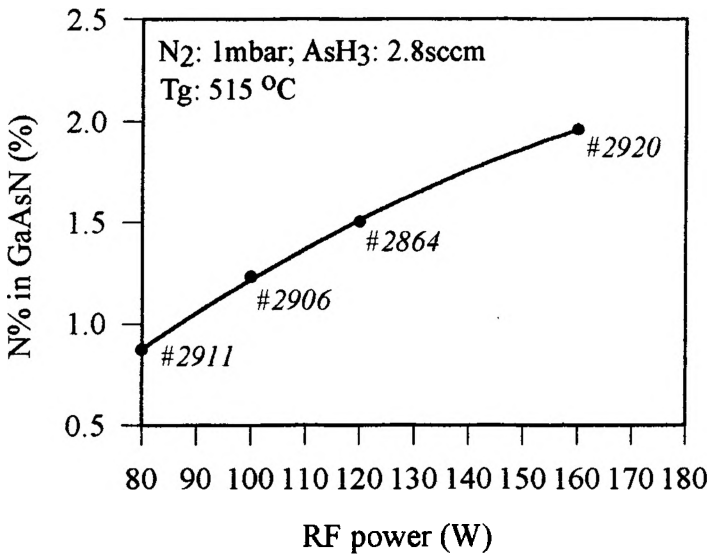

Fig.5.2 Effect of RF plasma power on N incorporation in GaAsN

matched to the GaAs substrate. The results of N incorporation in GaAsN versus RF power are shown at figure 5.2. The AsH_3 flow rate was 2.8sccm for all four samples. The input N_2 flow was kept constant for these samples (1.0mbar) and the RF power was the only parameter changed. N incorporation is seen to increase with increasing RF power. The relationship between the N concentration and RF power was close to linear, as reported by other groups[61]. The increasing N concentration in the GaAsN results from the production of more atomic N with increasing RF power as evident in figure 5.1(a). Figure 5.2 can be used as a calibration curve to estimate the expected N concentration at the chosen RF power between 80W and 160W when input N_2 flow is at 1mbar. This was found to yield consistent results for the N concentration determined by SIMS, as will be shown in chapter 8.

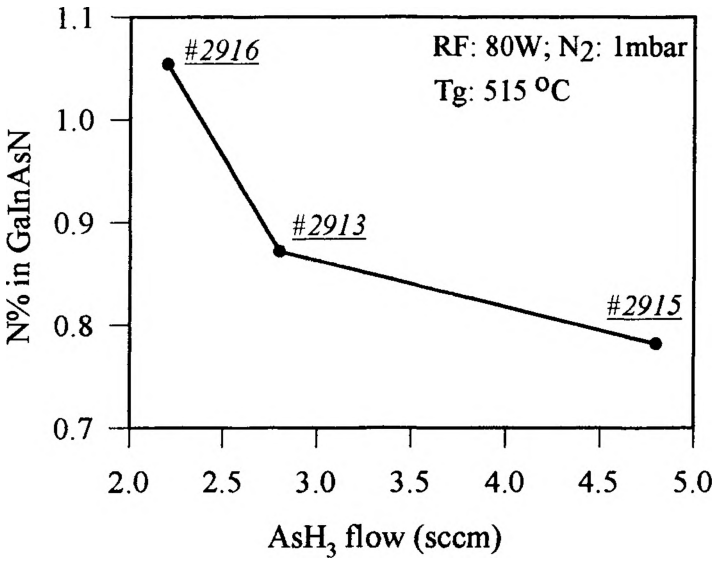

Fig.5.3 Effect of AsH_3 flow on N incorporation in GaInAsN QW with other growth conditions fixed

With RF power fixed at 80 W and the N_2 flow kept constant at 1 mbar, three GaInAsN QW samples (#2913, #2915, #2916) were grown for different AsH_3 flow rates. The growth structures consisted of a 70 Å GaInAsN QW sandwiched between 1500 Å GaAs barrier layers, and 250 Å InGaP outer barrier layers were grown to produce electron confinement to enhance the PL signal. All samples were covered by a 200 Å GaAs cap for annealing studies. The growth temperature for the GaInAsN QW was 515 ^{0}C, which was found to result in high quality InGaAs/GaAs QWs. The determination of the N concentration in GaInAsN QW was done by room temperature photoluminescence measurements. By comparing to a reference InGaAs QW with the same In content, the N composition in the GaInAsN QW was calculated from the PL peak shift such that 1%N

incorporation corresponds to a 150meV bandgap decrease[24], and this value is strain included. The relationship between the N concentration in the InGaAsN QW and the AsH_3 flow is shown in figure 5.3, with the AsH_3 flow changing from 2.2sccm to 4.7sccm. It was found that N incorporation decreased with increasing AsH_3 flow rate. This indicates that N and As compete in the incorporation process such that increasing the AsH_3 flow rate causes less N incorporation. In the later growths, unless specifically indicated, the AsH_3 flow rate was kept constant at 2.8sccm. Figure 5.4 shows the PL peak

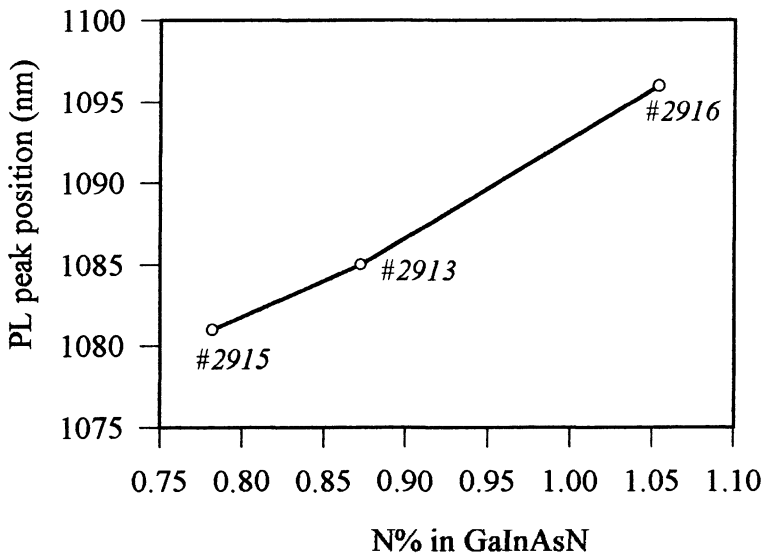

Fig.5.4 PL peak position shifts with N (%) in as-grown GaInAsN QW

position versus the N concentration in GaInAsN.

Thus the RF power, and the nitrogen input flow rate into the RF plasma source have a big effect on the N incorporation in GaAsN and GaInAsN. Higher nitrogen flows lead to more N incorporated in the Ga(In)AsN when all other growth condition are fixed. Although no systematic growth of GaAsN and GaInAsN was done to study N

incorporation in the sample, it could be inferred from figure 5.1(b) that N incorporation in GaAsN and GaInAsN should be proportional to the nitrogen input flow rate.

Several other factors such as substrate temperature and biasing were also adjusted to investigate their effect on the N incorporation into GaAsN and GaInAsN. Two substrate temperatures, 515 ^{0}C (#2906) and 480 ^{0}C (#2907), were used to grow GaAsN with all other growth conditions kept the same. Unlike the results reported by other groups[61,62], the N concentration in GaAsN materials were essentially unchanged, with 1.23% N in sample #2906 and 1.21% N in sample #2907. The probable reason was that the temperature difference we used was not very big (only 35 ^{0}C), while in reference 61, a temperature range of 100 ^{0}C (from 500 ^{0}C to 600 ^{0}C) was used. By biasing the substrate stage, the effects of charged ionized particles existing in the nitrogen plasma should be modified. Using +78V biasing on the substrate stage for the sample #2909, it should be possible to repel the positively charged ions. Sample #2907 was grown under the exact same conditions but without biasing. No significant effect of biasing on N incorporation was observed. The N composition in #2909, with biasing, is 1.17%, and in #2907, without biasing, is 1.21%. The difference between these values lies essentially within experimental uncertainty.

The On/Off control of N incorporation in GaInAsN QW was carried out with a mechanical shutter positioned between the RF plasma source and the substrate stage. In order to verify the effectiveness of the shutter, two samples (#2907, #2908) of GaAsN thick layers (1500 Å) were grown, one (#2907) with shutter open, the other one (#2908) with shutter closed. All the other growth conditions were the same. The sample structures consisted of a GaAs buffer layer (1000 Å) on the substrate, followed by the GaAs(N) epitaxial layer (1500 Å) of interest. The applied RF power was 100W, and the nitrogen

input pressure was 1.0 mbar. The resultant N concentration in GaAsN with shutter open (#2907) was 1.21%; i.e., the measured X-ray peak shift of the GaAsN epitaxial layer from that of the substrate GaAs is 630 arcseconds. However, if the shutter was closed, the X-ray peak of the epitaxial layer and the GaAs substrate were identical. This experimental result indicated that the shutter was completely effective in cutting off the active N from the plasma source.

CHAPTER 6

Unusual photoluminescence properties of GaInAsN quantum wells

In the current work, and for all examples reported in the scientific literatures, GaInAsN/GaAs quantum wells grown by MBE, MOCVD or OMVPE displayed much reduced photoluminescence compared to InGaAs/GaAs QWs. As more nitrogen is incorporated, the photoluminescence intensity of GaInAsN is steadily reduced and the linewidth increases. As a consequence much research is being undertaken in an effort to enhance the light output. In this work, the photoluminescence of a thick, 1500Å, layers of GaAsN material was undetectable, even at low temperature (16K), whereas light could be detected from quantum well samples. This chapter describes photoluminescence studies of GaInAsN/GaAs quantum well structures, grown using either the ECR plasma source or the RF plasma source. It was found that the photoluminescence could be greatly improved by thermal annealing. The optimum anneal condition has been determined.

6.1 Photoluminescence of GaInAsN QWs grown using an ECR source

Initial experiments employed an ECR plasma source to produce the active nitrogen for the growth of GaInAsN QW structures. Both ammonia (NH_3) and N_2 were used as the source gas for creating active N. The results of N incorporation using NH_3 were not reproducible. The use of N_2 was much more successful in growing GaInAsN QW samples.

Using N_2 as the source gas for the ECR source, three GaInAs(N) QW samples (#2680, #2681, #2682) were grown with the same structure but different N concentrations in the GaInAs(N) QW layer. All had the same In/Ga ratio (0.18 : 0.82). The basic growth structure of these samples is shown in figure 6.1. The nitrogen plasma source was off during the growth of sample #2680, so the quantum well was actually InGaAs. This sample was used as a reference against which the photoluminescence could be compared

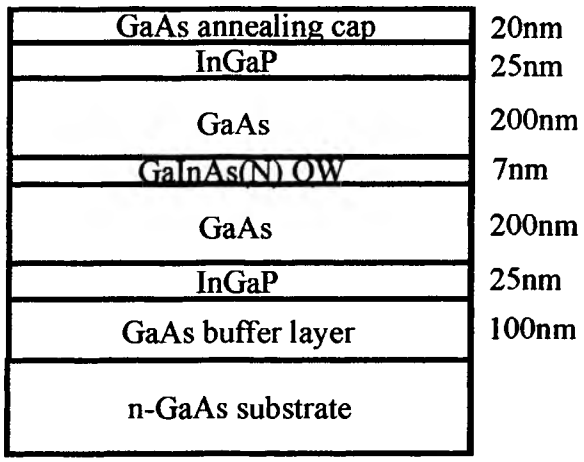

Fig.6.1 Schematic diagram of GaInAs(N) QW structure grown with ECR plasma source

following the addition of N. The difference between #2681 and #2682 was the N content in the GaInAsN QW. The content of N in sample #2681 was 0.3% and that in sample #2682 was 2.7%. All these three samples had the same AsH_3 flow rate (2.8sccm) and the QWs were grown at 520 ^{0}C. The use of InGaP layers in these samples was to create an effective electron-hole collection basin in order to have better confinement of electron and hole pair in the barrier layer and have better consistency in PL intensity measurement[63].

We considered that some charged energetic ions might exist in the nitrogen ECR plasma which might produce defects in the GaInAsN layer reducing the PL emission. An attempt to reduce this was made, using a permanent magnet filter. We hoped this would eliminate some ions by deflecting them from their path toward samples. This filter was found to have negligible effect on the results.

Temperature dependent photoluminescence measurements were performed on the GaInAsN samples. The samples were measured as-grown and after anneal at 800 ^{0}C for 15 seconds. Figure 6.2 shows the room-temperature photoluminescence intensity

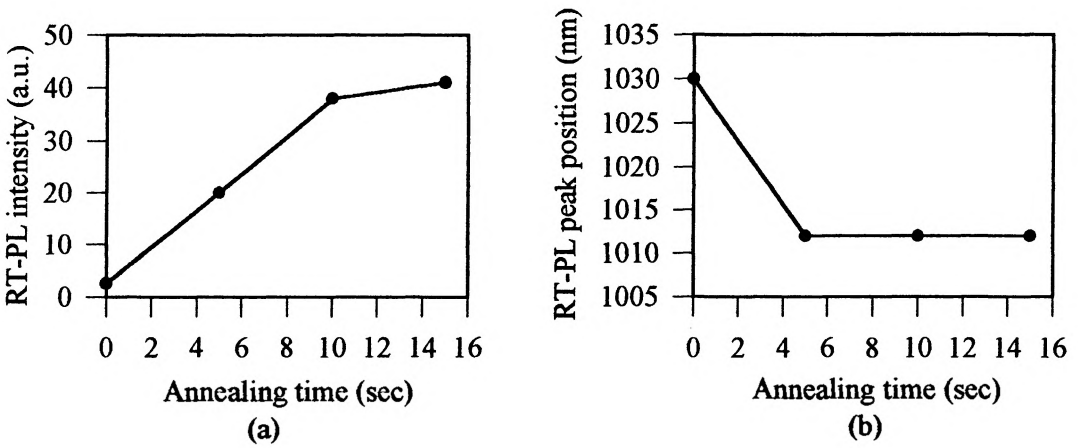

Fig.6.2 Effect of rapid thermal annealing at 800 ^{0}C on RT-PL intensity and induced blue shift of the peak position of GaInAsN (0.3%N) QW

improvement and a blue-shift of the peak position of the sample with 0.3% N after this anneal treatment. For the GaInAsN sample with 2.7% N content, PL could not be detected, even at low temperature 11K. However, after annealing, the PL signal of this sample was easily observed at all temperature up to 300K. Figure 6.3 shows the variation of the photoluminescence peak positions shift as the temperature is varied over the

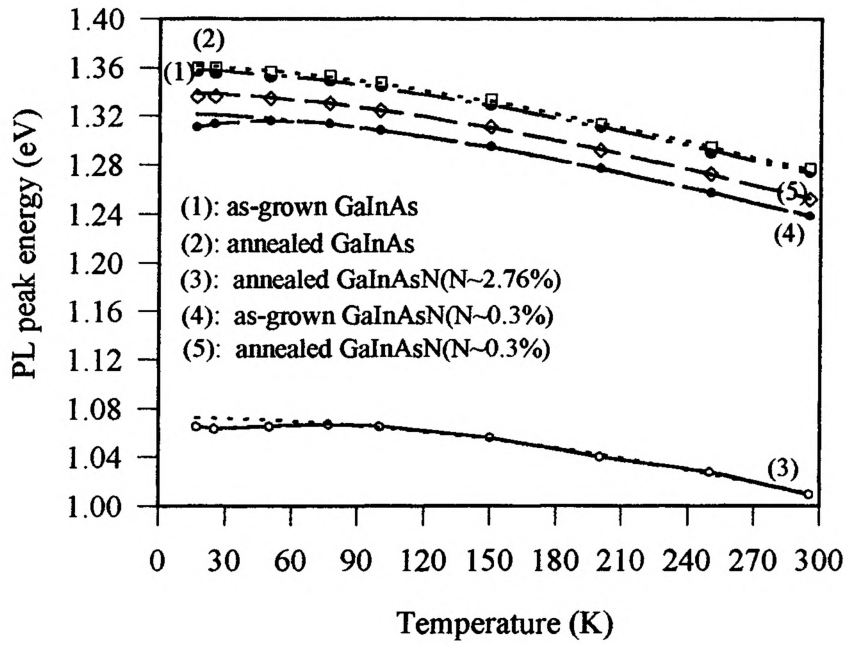

Fig.6.3 PL peak position vursus temperatures for as-grown and annealed GaInAs(N) QWs, the dots are measurement results, dashed lines are fitting from Varshni equation

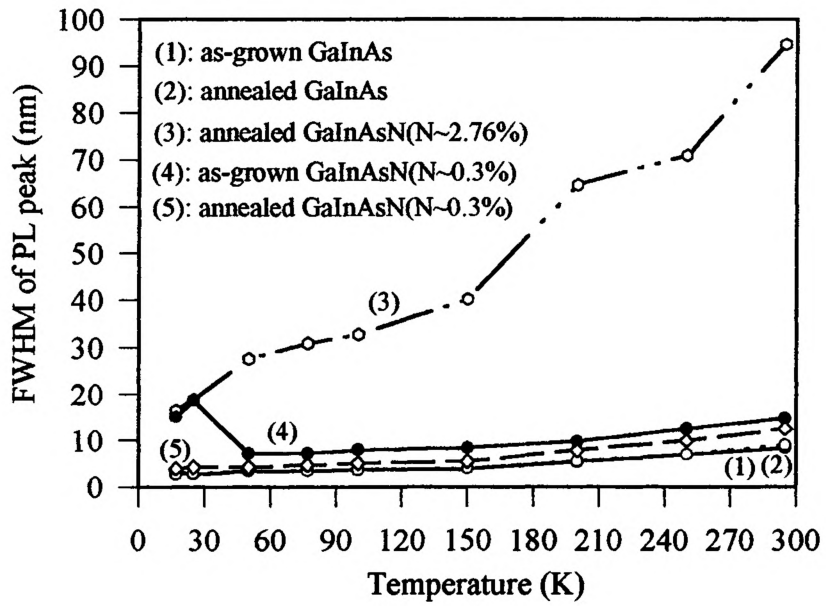

Fig 6.4 FWHM of the LT-PL peak of as-grown and annealed GaInAs(N) QWs

range 11~300K for as-grown and annealed GaInAsN (N~0.3% and ~2.7%) and the reference GaInAs QW samples. The various points in figure 6.3 are measurement results, and the dashed lines are fitting curves from the Varshni equation. The deviation from the Varshni equation (refer to curves 3 and 4 in fig.6.3) at very low temperatures (<50K) suggests the presence of phase separation[82]. In the reference sample the Vashini equation fits the data well over the entire temperature range. Figure 6.4 shows the FWHM of the PL emission peak of these samples. Generally, for the as-grown GaInAsN samples, N incorporation results in a low PL intensity and a wide FWHM of the PL peak. As the N content increases, the quality of GaInAsN drops rapidly. The reasons may be due to ion damage from the ECR plasma forming deep level defects; spinodal decomposition of GaInAsN; and group-V vacancy formation due to the decomposition of the weaker In-N bond relative to the Ga-N bond[16]. These factors together with non-optimized growth conditions may cause non-radiative recombination centers to be formed in the epitaxial layer.

From figures 6.3, and 6.4 and the curve of PL intensity versus temperature from 11K to 300K (not shown here), it is seen that the PL properties of the GaInAsN/GaAs QW are significantly improved by the anneal, while for the InGaAs QW, annealing had little effect on either intensity or peak position. For a GaInAsN QW, the PL peak intensity increased and the FWHM decreased after the anneal. This suggests that non-radiative recombination defect centers may be present in the as-grown QW film that are removed on anneal, or that the interface between QW and barrier may initially be rough and that annealing can smooth this interface. Also, a large blue shift (15meV) of the PL peak was observed in $Ga_{0.82}In_{0.18}As_{0.997}N_{0.003}$ due to the anneal, while the GaInAs only exhibited a shift of about 3meV. The large blue shift of the PL peak of GaInAsN is consistent with a high grown-in defect[33] concentration enhancing interdiffusion between

the GaInAsN QW and GaAs barrier layers during the anneal. The smaller effect seen for InGaAs QW may be due to the lower defect concentration present in this layer.

For the as-grown GaInAsN QW sample with 0.3% N composition (#2681), the PL peak splits into two peaks for T<50K (shown in figure 6.5) with a longer wavelength peak developing. As T decreases to below 20K, the intensity of the longer wavelength

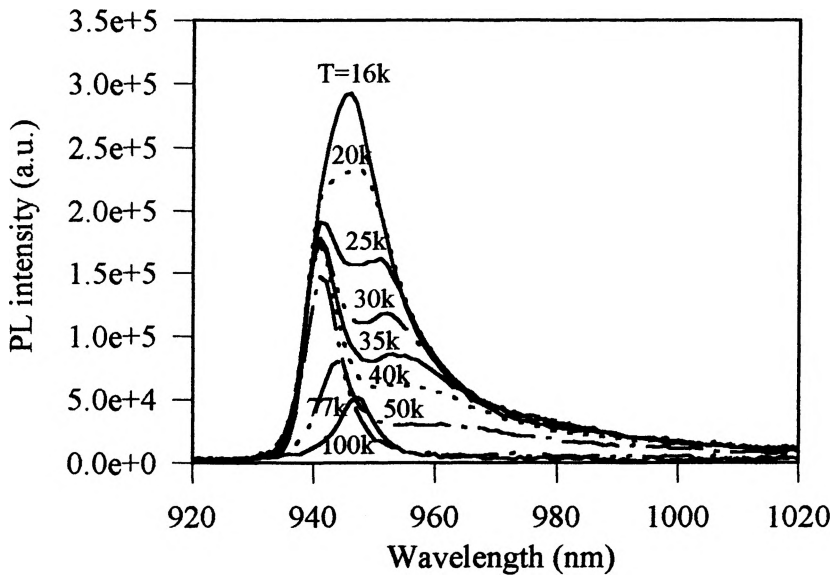

Fig.6.5 LT-PL spectra of as-grown GaInAsN (0.3%N) grown using the ECR source

peak increases and dominates over the shorter wavelength peak, but for T greater than 77K, the situation was reversed. However, after annealing, only a single PL peak was observed even at very low temperature of 11K and at a low laser pumping level. A plot of the LT-PL peak positions versus temperature is shown in figure 6.6 for both peaks. The shorter wavelength peak can be fit to the Varshni equation except below ~50K while the

longer wavelength peak increases almost linearly with T and has a much steeper slope than the Varshini equation at higher temperature. Therefore, we attibute the peak on the short wavelength side to band-band transitions, while the peak on long wavelength side may result from a certain energy level existing within the energy bandgap. But the

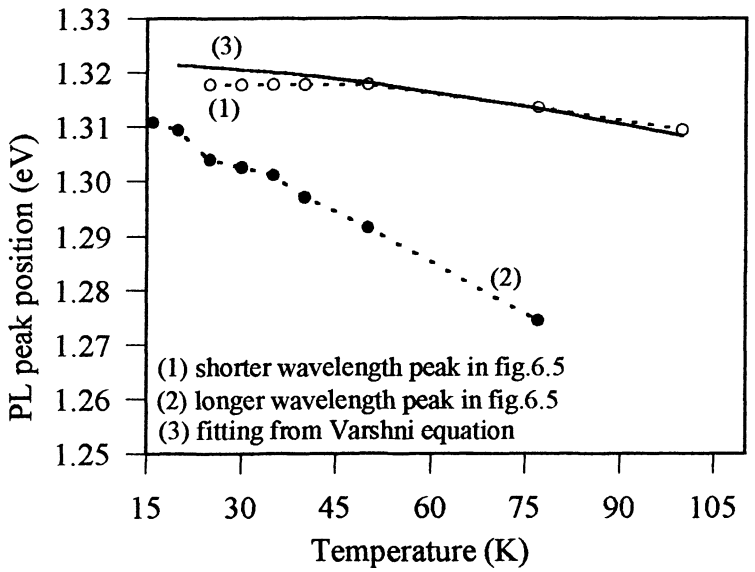

Fig.6.6 The effect of temperature variation on the PL peaks as shown in fig.6.5, the solid line is the same fitting curve from Varshni equation as in fig.6.3 and the dashed lines are only guide for eyes

mechanism is not clear now.

After annealing at 800 ^{0}C for 15 seconds, the PL behavior changes such that only a single peak is observed. The peak intensity increased and the linewidth narrowed.

6.2 Photoluminescence of GaInAsN QW grown using an RF source

As an alternative to using the ECR-N_2 source, an RF plasma source with N_2 was used to grow a GaAsN layer and GaInAsN QWs. This source proved to yield better results (i.e. better PL signal) than the ECR source.

6.2.1 Photoluminescence of as-grown GaInAsN QWs

Using N_2 as the source gas for the RF plasma source, GaInAsN QW samples were grown using various plasma conditions. The structure of GaInAsN QW samples grown is shown in fig. 6.7 and includes a GaInAs reference QW. This structure is designed to optimize the PL and is expected to result in better equivalence of the In/Ga ratio between the GaInAsN and the GaInAs reference because of the same MBE growth.

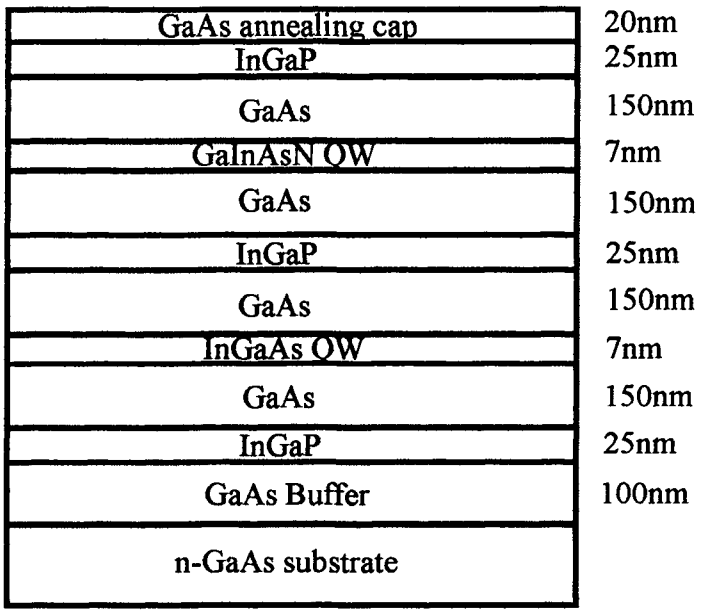

Fig.6.7 Schematic of GaInAs(N) QW grown using radio frequency plasma source

Similar to the growths with the ECR source, the PL intensity drops rapidly with increasing N content in GaInAsN, and the linewidth broadens. Thus, incorporation of N generally degrades the PL properties. Although we did not grow GaInAsN QW samples with the same N and In content using both ECR and RF plasma sources, it is still possible to draw comparisons between QW's grown using the different sources. Two significant differences are observed for the as-grown samples. For a $Ga_{0.82}In_{0.18}As_{0.9913}N_{0.0087}$ QW sample grown using the RF source, it was possible to observe PL at room temperature, whereas for a $Ga_{0.82}In_{0.18}As_{0.9966}N_{0.0034}$ QW grown using the ECR source (i.e. with less N) the room temperature PL signal was very weak. This indicates that the crystal quality of GaInAsN QW grown using the ECR source was poorer than that grown using the RF source even though it contained less nitrogen. This improvement of the PL quality of GaInAsN grown using RF source is ascribed to the fact that much less energetic N_2^+ is present in the RF plasma[38].

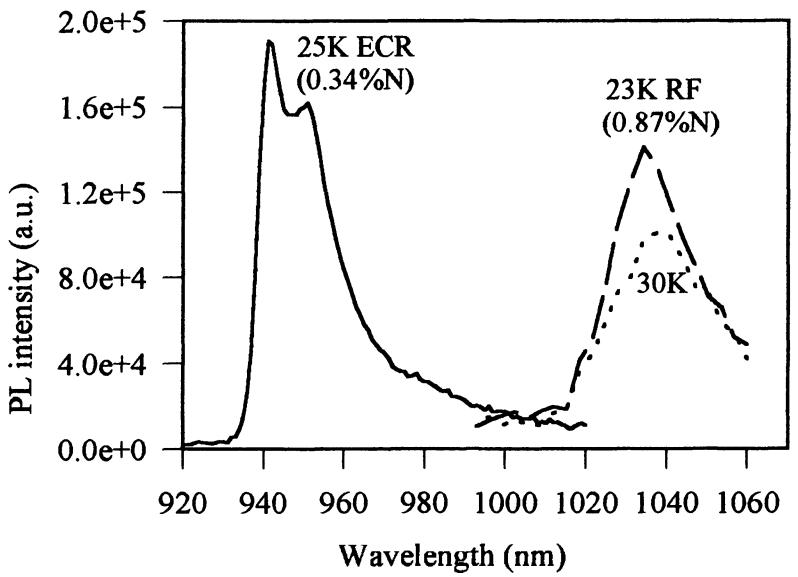

Fig.6.8 LT-PL of as-grown GaInAsN QW grown using RF and ECR plasma sources

The other difference observed for as-grown GaInAsN QW grown using two different plasma sources is in the low temperature photoluminescence measurement. As shown in figure 6.5, there are two PL peaks existing for $Ga_{0.82}In_{0.18}As_{0.9966}N_{0.0034}$ QW grown using the ECR source; however, for the $Ga_{0.82}In_{0.18}As_{0.9913}N_{0.0087}$ QW sample grown using the RF source, only a single broad (larger FWHM) peak is observed, as shown in figure 6.8. This could be because the two peaks in the higher N concentration, RF-grown samples merge together or that the microscopic variation in the N concentration is higher.

6.2.2 Annealing studies of GaInAsN quantum wells

Since rapid thermal annealing resulted in a significant improvement in PL intensity for ECR-grown samples, a more systematic annealing study was carried out on the RF-grown samples. The N content in the GaInAsN QW was varied by changing the RF power and AsH_3 flow. The N concentration in the GaInAsN QW was determined by the red shift of PL peak relative to the reference InGaAs QW using a calibration of 150meV/%N.

Four samples with N concentrations of: (1) 0.87%, (2) 0.78%, (3) 1.05%, and (4) 1.25% were grown. The variation of N content for (1) and (4) was obtained by changing the RF power, while the variation of N content for (1), (2) and (3) was obtained by changing the AsH_3 flow. The PL intensity of the as-grown InGaAs QW was ~450 times greater than that of GaInAsN sample with 0.87%N. Generally, the PL intensity of the as-grown GaInAsN QWs decreases with increasing N content. However, for the case of curves (1) and (2), although the N content of (2) is slightly less than that of (1), the PL intensity of (2) is lower than that of (1). This might be due to the fact that the AsH_3 flow

of the former (~4.7sccm) was higher than that of the latter (~2.8sccm), and a too high an AsH_3 flow might result in excess As incorporation and slightly poorer optical quality of GaInAsN QW.

The samples were annealed at 600 ^{0}C - 850 ^{0}C. Annealing at 600 ^{0}C and 650 ^{0}C showed no change in the PL quality of GaInAsN QWs. Annealing at too high a temperature (e.g. 850 ^{0}C) resulted in surface damage of the GaInAsN samples, which destroyed the PL yield. Some black/brown spots formed on the surface and were easily observed under the microscope after annealing at 850 ^{0}C. The impact of anneals at temperatures of 700 ^{0}C, 750 ^{0}C and 800 ^{0}C for various annealing times on the PL intensities is shown in figure 6.9 for four samples with different N contents. The plots of annealing induced peak position shifts as a function of anneal times are seen in figure 6.10. Although arbitrary units are used for the PL intensity in figure 6.9, the measured PL intensities are comparable for the three graphs as a result of a fixed laser pump power density and a fixed measurement set-up. Therefore, the increase of the PL intensities was ascribed to annealing factors. Referring to figures 6.9 and 6.10, it can be seen that the PL intensity improvement is associated with the blue-shift of the peak wavelength. After the PL intensity reaches saturation, little additional blue-shift is produced. It can also be seen that the PL intensity and wavelength changes after anneal occur in much shorter times at the highest anneal temperatures. For a 700 ^{0}C anneal it takes about 120 min for the PL intensities and blue-shift to reach the maximum values. This is shortened to ~5 seconds at 800 ^{0}C. For times > 10 s at 800 ^{0}C, the PL intensity drops off, this may be due to surface decomposition effects.

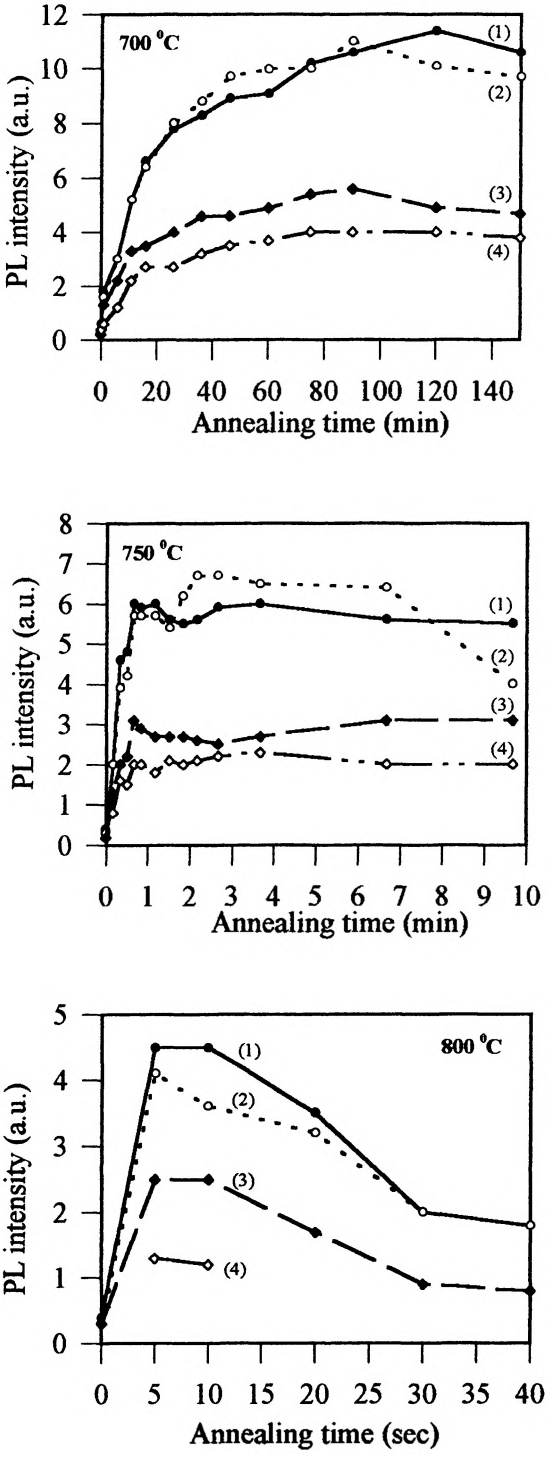

FIG.6.9 PL intensities versus annealing time at (a) 700 ^{0}C, (b) 750 ^{0}C, (c) 800 ^{0}C; N concentrations are (1) 0.87%, (2) 0.78%, (3) 1.05% and (4) 1.25%

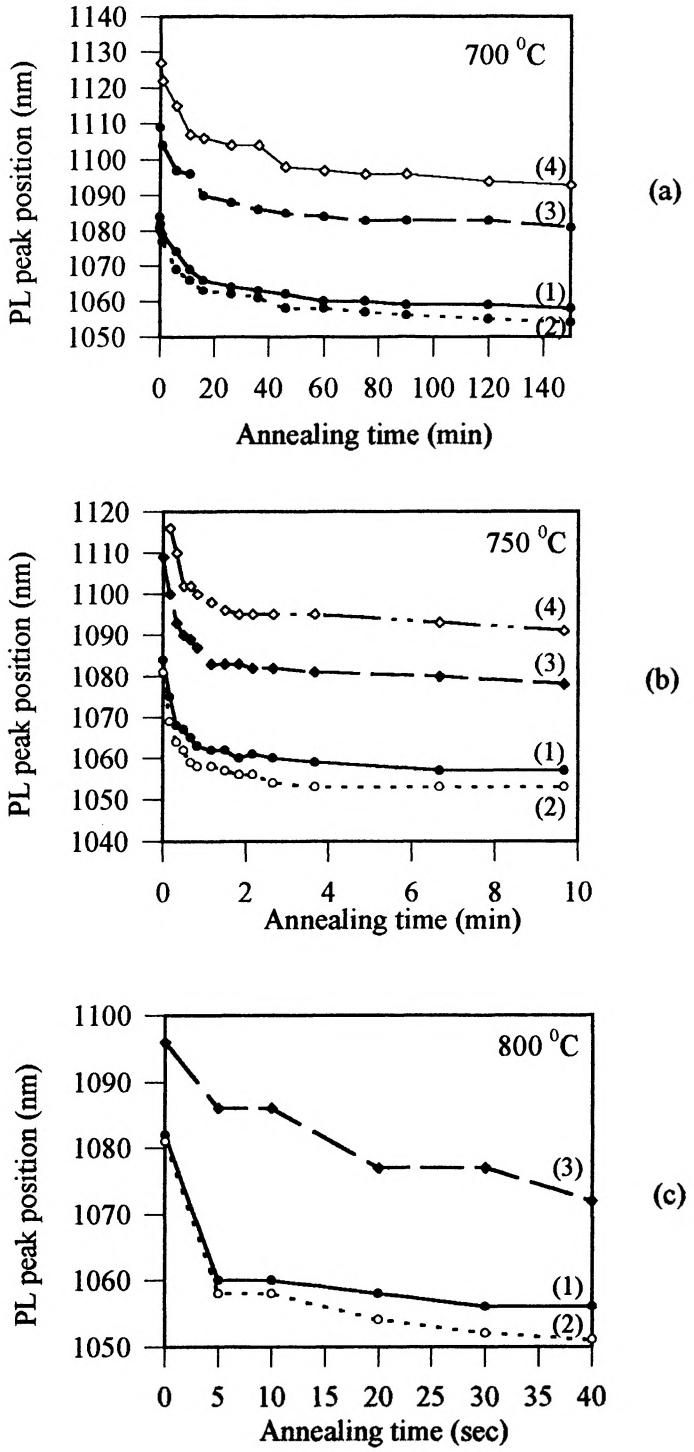

Fig.6.10 PL peak position red-shift as a function of annealing time for 700 °C, 750 °C and 800 °C, the N concentrations are:(1) 0.87%, (2) 0.78%, (3) 1.05% and (4)1.25%

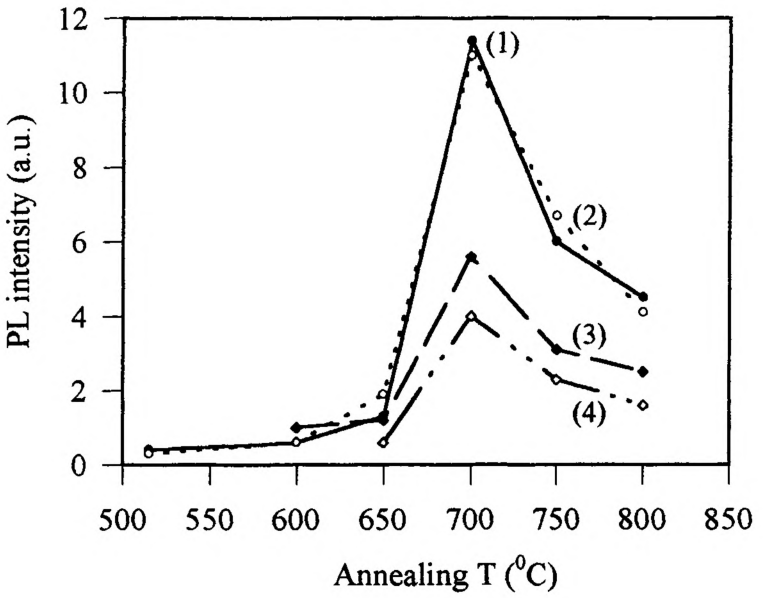

FIG.6.11 The maximum PL signal intensities after anneal at different T; N concentrations are: (1) 0.87%, (2) 0.78%, (3) 1.05% and (4) 1.25%

The maximum intensities reached after anneal at the different temperatures are summarized in figure 6.11. Clearly, annealing at 700 ^{0}C results in the best PL intensity at all N-contents, but it requires a long time to achieve the maximum (>1hr). Under all the anneal conditions, the InGaAs reference QWs exhibited little change. Also as seen in figure 6.12 the samples show a large blue-shift in the PL peak wavelength for anneal between 650 - 750 ^{0}C. The peak position for certain temperatures in figure 6.12 is obtained at its optimum annealing time when the maximum PL intensity is reached. Above 750 ^{0}C the QWs with the highest N content exhibit a red-shift in the PL wavelength. From figures 6.11 and 6.12, it appears that a mechanism is activated at temperatures between 650 ^{0}C to 700 ^{0}C, which results in the increase of the PL intensity

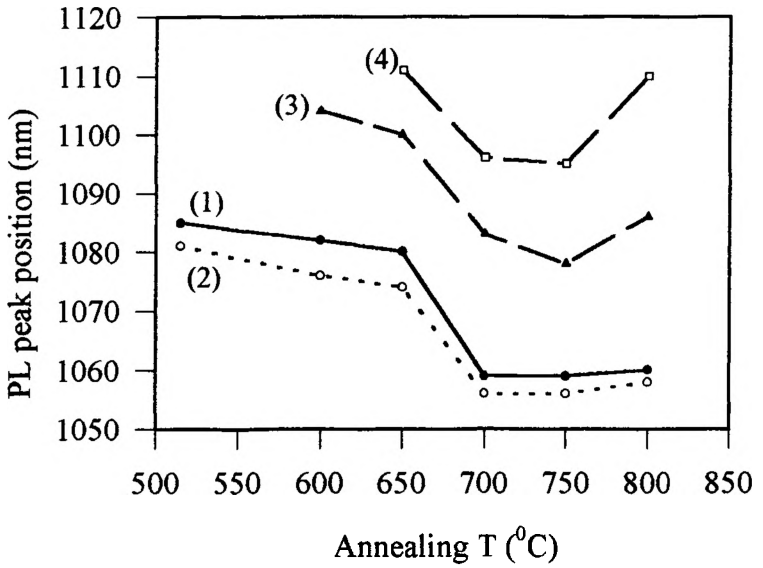

FIG.6.12 Shift of PL peak wavelength versus annealing temperatures, N concentrations are: (1) 0.87%, (2) 0.78%, (3) 1.05% and (4) 1.25%

and a wavelength blue-shift. This blue-shift associated increasing of PL intensity might be due to the migration of grown-in defects. The diffusion of defects through the quantum well/barrier interfaces and out of the QW account for the improved PL and blue-shift. Larger blue-shifts of the PL peak wavelength of GaInAsN than that of InGaAs QW after annealing indicates that the diffusion coefficient of In-Ga interdiffusion for GaInAsN is much larger than that for InGaAs, and the diffusion coefficient also increases with increasing N content in GaInAsN. This might be due to the fact that interdiffusion is enhanced by the presence of crystal defects[33]. Another possible reason causing PL peak blue-shift after annealing is that some N might diffuse out of the quantum well and lead to a decreasing of N concentration in QW. When the annealing temperature is further increased, a competing mechanism such as exhaustion of defects is activated, which limits the increase of the PL intensity, this leads to saturation of the PL intensity and little

additional blue-shift. At the higher annealing temperatures, the second mechanism becomes more significant. This could explain why the saturation of the PL intensity of annealed GaInAsN QW samples is observed much earlier at 750 ^{0}C than that at 700 ^{0}C. The second mechanism looks as if a finite number of grown-in defects get exhausted when the annealing temperature becomes higher. However, the results of Hall effect measurements on annealed GaInAsN in chapter 8 indicate that there are still a large number of electron and hole traps existing in the annealed GaInAsN materials. The nature of the defects in GaInAsN and their roles to annealing are not yet understood. The origin of the red-shift of the PL peak wavelength after annealing at 800 ^{0}C for sample (3) and (4) is not known, it is possibly due to the formation of N clusters in the material.

An in-situ anneal in the environment of an As_2 overpressure in the MBE chamber was also performed at 620 ^{0}C for 1 hour. No significant improvement of PL intensity was observed compared to the as-grown sample. This might be because the annealing temperature is not high enough as indicated in figures 6.11 and 6.12. Further post-annealing was carried out on this in-situ annealed sample in the environment of flowing N_2 in the RTA furnace. The improvement of the PL intensity was found to be very similar to that after annealing of the as-grown sample (1) in figure 6.11.

CHAPTER 7
Spinodal decomposition of GaInAsN and GaAsN

Spinodal decomposition arising from the lattice mismatch of binary constituents in the ternary and quaternary compound results in composition fluctuations of the material. This is thought to be one of the main reasons for the poor optical quality of Ga(In)AsN materials[67, 68]. In this chapter, the calculation of the miscibility gap of GaAsN is described, and TEM micrographs showing evidence of spinodal decomposition in GaInAsN QWs are provided.

7.1 Theory of spinodal decomposition

A miscibility gap is an unstable solid phase composition domain at a certain temperature. For the materials GaInAsN and GaAsN, a miscibility gap exists due to a large difference in the lattice constants of the binary components. Stringfellow's[41] delta lattice parameter (DLP) model, based on the dielectric theory of Philips[42] and Van Vechten[43], has been shown to be suitable for calculating the miscibility gap for both quaternary and ternary bulk material systems. A critical temperature is defined, above which complete miscibility occurs and homogeneous crystals can be grown. The spinodal curve can be calculated from the total free energy of the material system G(x,y) using the following equation for ternary materials[44]:

$$\frac{\partial^2 G}{\partial x^2} = 0$$

and for quaternary materials:

$$\frac{\partial^2 G}{\partial x^2}\frac{\partial^2 G}{\partial y^2} - \left(\frac{\partial^2 G}{\partial x \partial y}\right)^2 = 0$$

where G is the total free energy per mole and (x,y) are the composition ($Ga_{1-x}In_xAs_{1-y}N_y$).

The total free energy G consists of two terms: Gibbs free energy per mole G^s and the strain energy G^{str}. For ternary materials, G^s can be expressed as[41]:

$$G^s = -Ka_0^{-2.5} + RT[x\ln x + (1-x)\ln(1-x)]$$

while for quaternary materials $A_{1-x}B_xC_yD_{1-y}$:

$$G^s = -Ka_0^{-2.5} + RT[x\ln x + (1-x)\ln(1-x) + y\ln y + (1-y)\ln(1-y)]$$

where R is the gas constant, T the absolute temperature, x and y the composition, a_0 the lattice constant, and K a constant [$1.15\text{x}10^7$ cal/(mol·Å$^{2.5}$)].

The strain energy always stabilizes the materials system against infinitesimal compositional fluctuations and reduces the critical temperature[44]. There are two ways to consider the strain energy. If the epitaxial layer of the material is lattice matched to the substrate and it is strain free before spinodal decomposition, one can use Cahn's method by including the coherency strain into the stability criterion by a simple expression[44]. However, GaInAsN may be highly strained (the In content of interest is between 18% to 30%, and the strain, Δa/a, is up to 2%), so it is necessary to use Lazzari's method by including the strain effect of the substrate into the miscibility gap calculation[45]. Using Lazzari's method, the strain energy G^{str} caused by the lattice mismatch between epitaxial layer and (100) GaAs substrate is given by:

$$G^{str} = V_m \frac{E}{1-\gamma}\varepsilon^2$$

or

$$G^{str} = V_m \frac{(C_{11}-C_{12})(C_{11}+2C_{12})}{C_{11}}\left[\frac{a_{(x,y)}-a_0}{a_0}\right]^2$$

where E is Young's modulus, γ the Poisson ratio, C_{11} and C_{12} the elastic constants, ε the strain, a_0 and $a_{(x,y)}$ the lattice constants, and V_m the molar volume. All of the parameters C_{ij}, E, γ, and a_0 can be calculated from the parameters of the binary constituents using

Vegard's Law. By solving the above equations, the miscibility gap calculation of ternary or quaternary materials can be obtained.

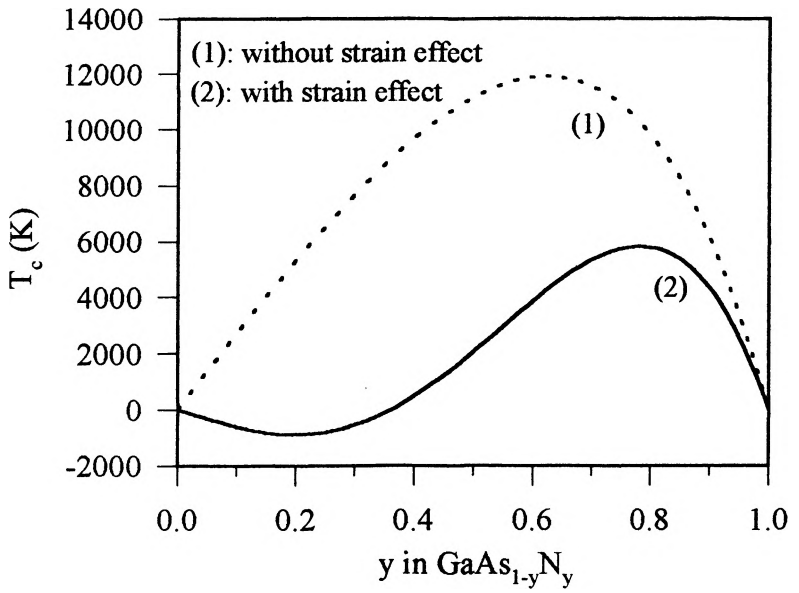

Fig.7.1 Calculated miscibility gap of $GaAs_{1-y}N_y$, the dash line is calculated without consideration of strain energy, and the solid line with consideration of strain energy

The results of the calculated miscibility gap for $GaAs_{1-y}N_y$ are shown in figure 7.1. The x- axis is the nitrogen concentration in GaAsN, and the y- axis is the critical temperature. T_c is defined as that any growth temperature higher than Tc, spinodal decomposition will not occur, otherwise, spinodal decomposition will exist in the epitaxial layer. The negative critical temperature at some composition ranges means that the material is stable at all practical growth temperatures and no miscibility gap exists. Once the nitrogen composition has been decided, T_c can be obtained from figure 7.1, and practical growth temperature should be greater than T_c in order to avoid the spinodal decomposition. Curve (2) in figure 7.1 is obtained after considering the strain energy, and it lowers the critical temperature dramatically. Due to the large difference of the lattice

constant of the binary constituents of GaAsN, the validity of the dielectric theory for this material system has been questioned [46]. However, some researchers have experimental reports[23, 47] that the band gap energy of GaAsN with small nitrogen content is in good agreement with predictions from the dielectric theory. Fortunately, the content of N in GaAsN of interest for near infrared lasers is only a few percent, so that the theory description of this nitride at low N concentrations is appropriate.

Theoretical calculations for the GaInAsN material can also be done. However, the mathematical calculation is much more complicated. The results of the miscibility gap in GaInAsN were obtained in reference 69.

7.2 Experimental demonstration in Transmission Electron Microscopy

In order to analyze the spinodal decomposition structure in GaInAsN QWs, cross-sectional transmission electron microscopy (TEM) was employed. Two single quantum well samples were first grown with the structure as shown in figure 6.1. One contained a N-free InGaAs QW, the other is GaInAsN QW with 2.7%N. TEM samples of GaInAsN and GaInAs cut along both the [0 -1 1] and [0 1 1] directions were prepared by mechanical polishing and subsequent thinning by ion milling to reach a thickness between 100nm and 200nm. Two diffraction vectors, **g**=022 and **g**=400, were used for the analysis of the [0 -1 1] direction, and **g**=0 -2 2 and **g**=400 were used for samples with [0 1 1] direction.

Figure 7.2 shows cross-sectional TEM micrographs using diffraction vectors **g**=022 for the as-grown GaInAsN (N~2.7%) and GaInAs QWs cut along the [0 -1 1] direction. The diffraction condition at **g**=022 is sensitive to the compositional modulations along the [0 -1 1] direction. The compositional modulation due to the spinodal-like decomposition occuring during the growth causes non-uniform strain

(a)

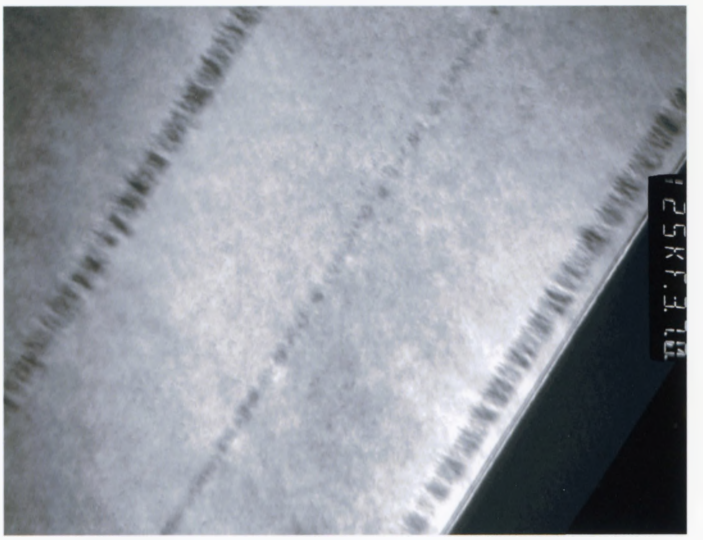

(b)

Fig.7.2 The dark-field cross-sectional TEM micrographs using diffraction vector **g**=022 for the as-grown (a) GaInAs QW, and (b) GaInAsN (N~2.7%) QW, the magnification is 125K

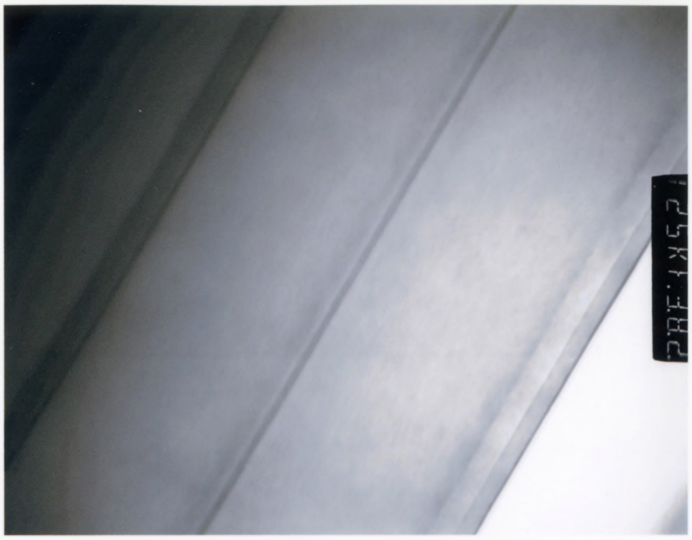

(a)

(b)

Fig.7.3 The bright-field cross-sectional TEM micrographs using diffraction vector **g**=400 for the as-grown (a) GaInAs QW, and (b) GaInAsN (N~2.7%) QW, the magnification is 125K

inside the QW material. This non-uniform strain leads to bending of the local lattice plane at the free surface of the foil, which causes a strong black and white contrast image. Figure 7.3 are the cross-sectional TEM micrographs using diffraction vectors **g**=400 for the as-grown GaInAsN (N~2.7%) and GaInAs QWs cut along the [0 -1 1] direction. The lower contrast modulation observed for **g**=400 in the [0 -1 1] direction indicates that these planes are elastically strained by the surrounding materials. In our TEM studies of the GaInAsN sample, there is no essential difference observed in the microscopy images between the [0 -1 1] and [0 1 1] directions under the diffraction condition of **g**=022 and **g**=0 -2 2, respectively (figures not shown here). However, comparing samples of GaInAsN and GaInAs QWs using the same **g**=022 diffraction condition, it is found that the contrast modulation is stronger for the GaInAsN sample than that of GaInAs. This means that compositional modulation becomes stronger with N incorporation into the GaInAs QW, even though the total strain is reduced due to the smaller atomic size of N. Figure 7.4 shows higher magnification (200K) TEM micrographs of the same samples as in figure 7.2 and for the **g**=022 diffraction vector. It is obvious that the GaInAsN sample containing 2.7% N displays significantly more serious composition modulation than the GaInAs QW sample.

In order to better compare different GaInAsN and GaInAs QW samples, a three QW structures were grown. The schematic diagram of these three-QW structures is shown in figure 7.5. In this case, a N-free InGaAs QW, a GaInAsN (N~1.0%) QW, and a GaInAsN (N~1.7%) QW were grown in a single structure. Each quantum well is 70 Å thick and the wells are separated by 500 Å GaAs layers. Figure 7.6 shows the TEM result of this structure; fig.7.6(a) is obtained under the condition of **g**=022 and fig.7.6(b) is obtained with **g**=400. The magnification of figure 7.6 is large (x300K). Unfortunately, the thickness of this TEM sample seems still too thick, but it can

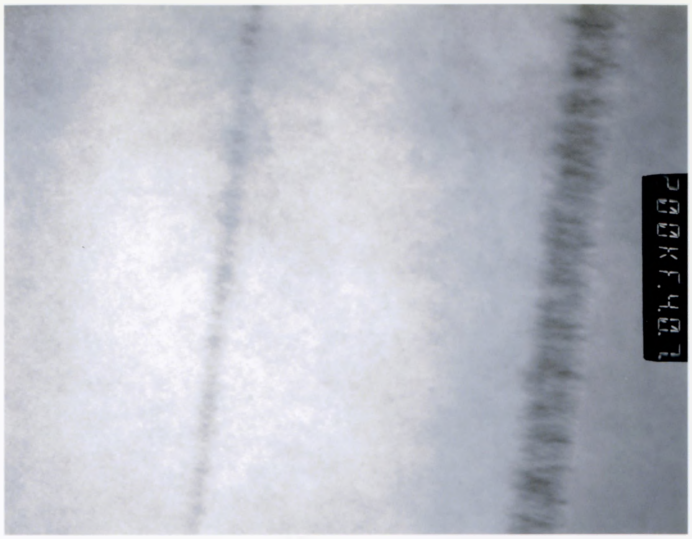

(a)

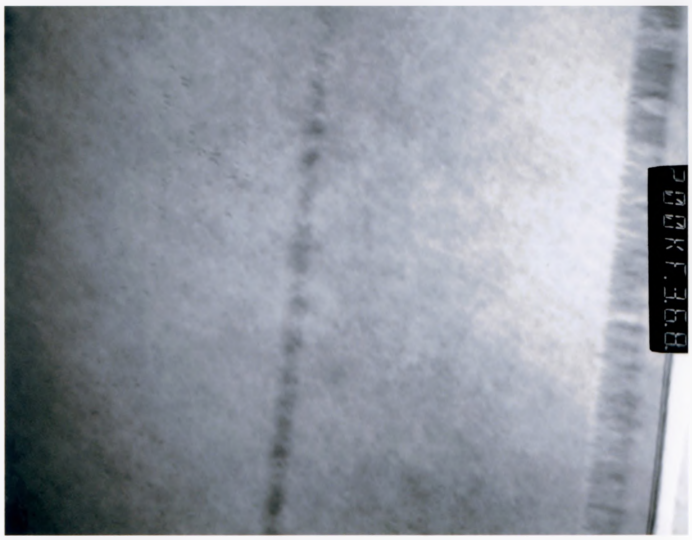

(b)

Fig.7.4 The bright-field cross-sectional TEM micrographs using diffraction vector **g**=022 for the as-grown (a) GaInAs QW, and (b) GaInAsN (N~2.7%) QW, the magnification is 200K

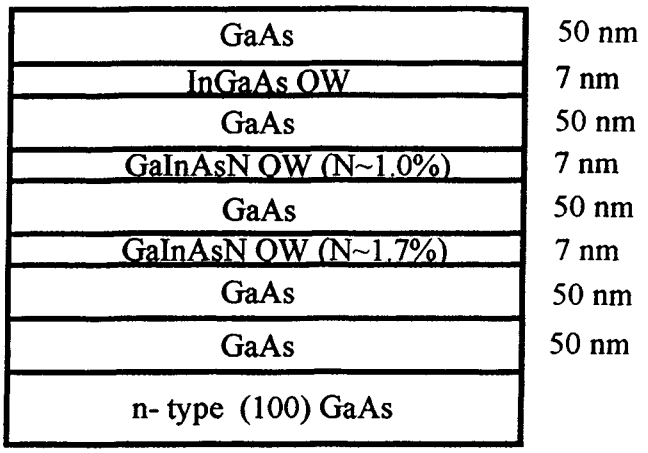

Figure 7.5 Schematic diagram of three-QWs structures for TEM studies

still be observed from figure 7.6(a) that the edge of the GaInAsN QW is more corrugated than that of GaInAs QW. This is consistent with the previous TEM observation for GaInAsN and InGaAs QWs on the different substrates. The TEM micrograph obtained with a g=400 diffraction vector displays sharp QW edges, uniform QW structures and there is no clear difference between GaInAsN and InGaAs QWs as we expected.

Figure 7.7(a,b) are TEM micrographs of a thick GaAsN layers. The structure is simply a 600 Å GaAsN (N~1.74%) epitaxial layer on a 1000 Å GaAs buffer layer. The substrate is (100) GaAs. Figure 7.7(a) is obtained with the diffraction vector g=022, and fig.7.7(b) is taken with g=400. Unlike the spinodal decomposition observed in GaInAsN with diffraction vector g=022, the thicker GaAsN epitaxial layer did not show any composition modulation, and the interface between GaAsN and GaAs is sharp as shown in figure 7.7(a). According to the theoretical prediction curve of figure 7.1, indeed, there should not be any phase separation occurring in GaAsN epitaxial layer with a N concentration of about ~1.7% and at any practical growth temperature

(a)

(b)

Fig.7.6 The bright-field cross-sectional TEM micrographs for as-grown 3QWs structure in figure 7.5, (a) using diffraction vector **g**=022, and (b) **g**=400, the magnification is 300K

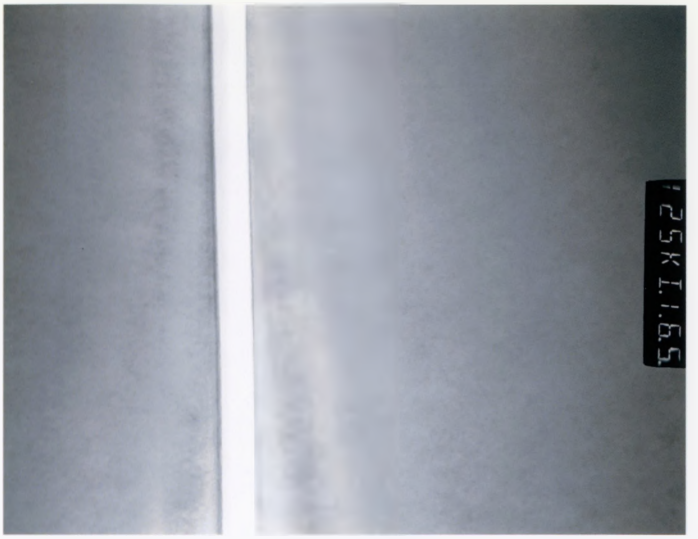

(a)

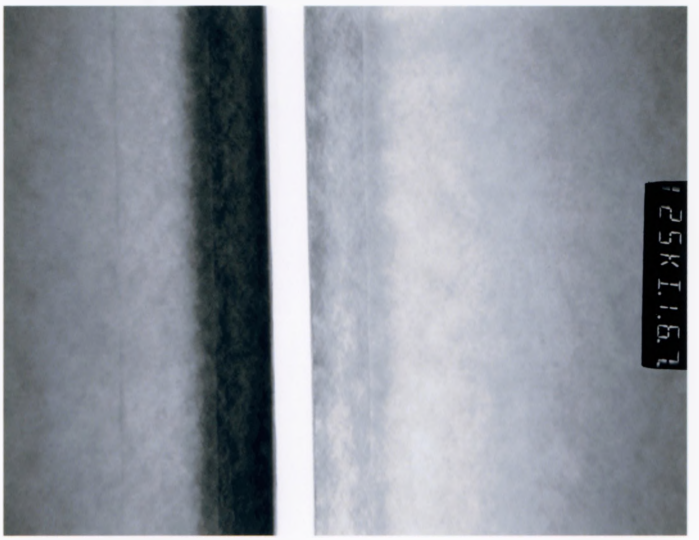

(b)

Fig.7.7 The bright-field cross-sectional TEM micrographs for a single GaAsN (600 Å, N~1.74%) layer structure, (a) using diffraction vector **g**=022, and (b) **g**=400, the magnification is 125K

since the critical temperature is negative in the whole low N concentration range.

Although no spinodal decomposition occurs in GaAsN epitaxial layer as demonstrated by TEM experiments, the photoluminescence measurements carried out on GaAsN revealed that the addition of N to GaAs significantly reduces the PL emission, even at N concentration less than 1%. This phenomenon indicates indirectly that in addition to the spinodal decomposition that might degrade the crystal quality of GaInAsN, there must exist other, more important factors, that are responsible for the poor PL quality of GaAsN and GaInAsN. This could be due to defects formed by the energetic ions or molecules in the nitrogen plasma, or other deep level defects formed by the process of N incorporation into GaAs or GaInAs but not related to the energetic species.

CHAPTER 8
Other characteristics of GaInAsN

As mentioned in chapter 6, the photoluminescence intensity of GaInAs decreases dramatically with the addition of a small amount of N. For comparison, the PL intensity of a nitrogen-free InGaAs QW was observed to be 450 times greater than that of GaInAsN with N~0.87% and the linewidth is much narrower. With increasing N, the PL intensity decreases and linewidth of the PL peak broadens. These results are not only observed in our GS-MBE grown material using a nitrogen RF plasma source, but also in GaInAsN samples grown by MOCVD[28, 32] where the active N is produced not by a plasma source but by the chemical reaction of dimethylhydrazine (DMHy). Actually, all the current reports of GaInAsN and GaAsN samples reveal poor photoluminescence qualities no matter what growth technique and active nitrogen source are used. Some possible explanations for the poor PL quality are: (1) spinodal decomposition of GaInAsN under normal growth conditions[17,18, 70], (2) defects formed in the material caused by ion damage by the plasma source[38], (3) group V vacancy production due to the decomposition of weaker In-N bonds[28], and (4) high concentration of contaminants (H,C and O) incorporated during the growth[28].

In order to identify possible contaminants, and to determine whether some of them are playing a role in the PL intensity reduction in GaInAsN epitaxial layers, secondary ion mass spectrometry (SIMS) was used in this work to analyze for H, O, B, C and Si. Also, the In and N concentrations were measured for comparison with the values determined by X-ray diffraction. The layers of Ga(In)AsN were also characterized by

room temperature Hall effect measurements. These were performed on un-doped, Si doped (nominally n = $4x10^{17}$ cm^{-3}) and Be doped (nominally p = $4x10^{17}$ cm^{-3}) GaInAsN epitaxial layers grown on semi-insulating GaAs substrates.

8.1 Experimental SIMS results of GaInAsN

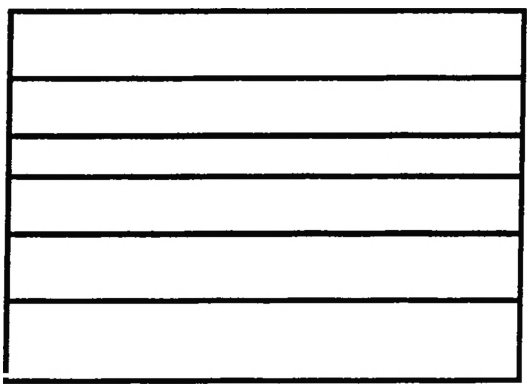

Fig.8.1 Schematic diagram of GaInAsN SIMS sample structure

The sample designed for SIMS measurement is shown in figure 8.1. The relative composition of In:N ≈3:1 leads to a GaInAsN epitaxial layer lattice matched to GaAs. The nominal composition of $Ga_{0.955}In_{0.045}As_{0.985}N_{0.015}$ was determined by X-ray diffraction. After growth of a 2000 Å $Ga_{0.955}In_{0.045}As_{0.985}N_{0.015}$ layer, a 500 Å $Ga_{0.955}In_{0.045}As$ layer was deposited with the shutter in front of the nitrogen plasma closed. The advantages of this kind of structure are: (1) by comparing the contaminants and their corresponding concentrations in the neighbor $Ga_{0.955}In_{0.045}As_{0.985}N_{0.015}$ and $Ga_{0.955}In_{0.045}As$ layers, it is possible to determine which contaminant is related to or accompanied by the N incorporation into GaInAs, (2) by measuring the N concentration

in $Ga_{0.955}In_{0.045}As$, it is possible to determine the effectiveness of the shutter in front of the N plasma. The growth of a QW sample requires a perfectly operating shutter, i.e. the shutter should block all the N from reaching the sample surface. After the growth of

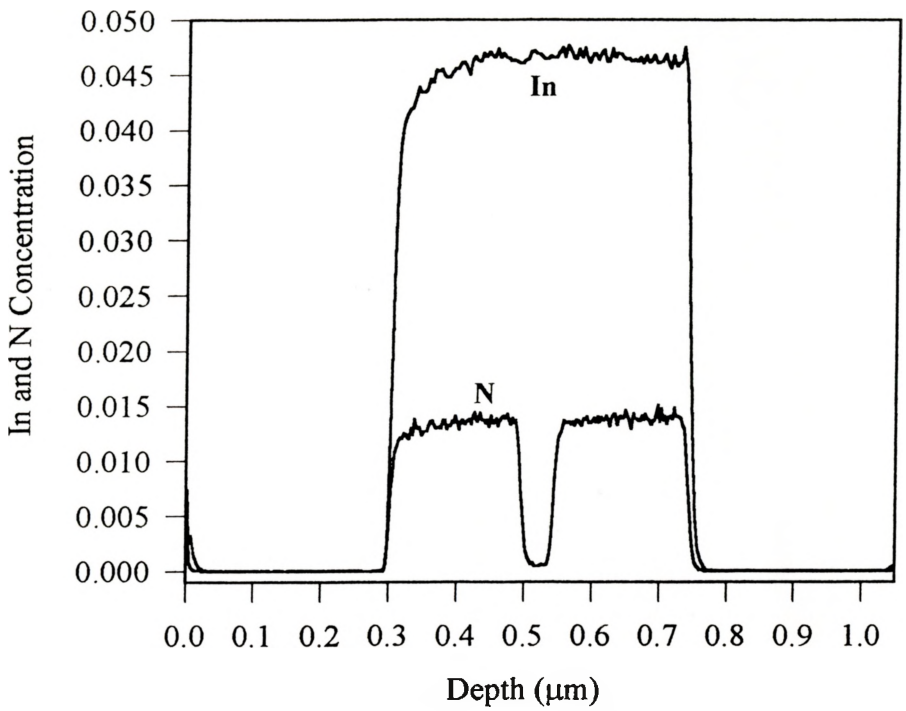

Fig.8.2 SIMS results of N and In concentration in GaInAsN structure as Fig.8.1

$Ga_{0.955}In_{0.045}As$, 2000 Å $Ga_{0.955}In_{0.045}As_{0.985}N_{0.015}$ was grown and the sample was finished with a 3000 Å GaAs layer. The GaInAs(N) epitaxial layers were grown at 515 ^{0}C. The background contaminants and their corresponding concentrations can be determined by SIMS in the GaAs epitaxial layer.

The measured depth distribution of In and N in the sample of figure 8.1 are shown in figure 8.2. For the SIMS measurement, the N concentration is calibrated against an

implanted standard sample, with a much lower N- concentration than our sample. The In concentration is calibrated against a layer of InGaAs lattice matched to InP, and therefore at a much higher concentration than our sample shown in figure 8.1. The measured N and In concentrations obtained from figure 8.2 agree well with the nominal values derived from the calibration based on X-ray diffraction. This indicates the validity of the X-ray diffraction techniques in the determination of constituent composition. Also, it is determined that the shutter is at least 98% effective. The constant In concentration where the growth changes from $Ga_{0.955}In_{0.045}As_{0.985}N_{0.015}$ to $Ga_{0.955}In_{0.045}As$, then back to $Ga_{0.955}In_{0.045}As_{0.985}N_{0.015}$ layer indicates that In incorporation is not affected by the presence of N.

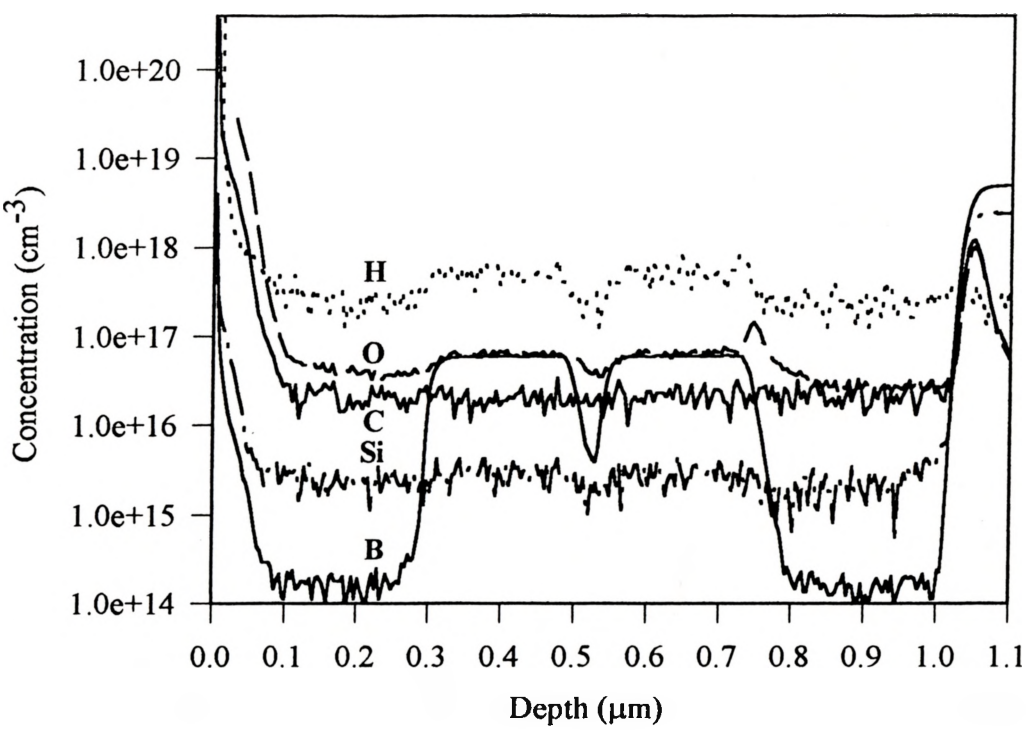

Fig.8.3 SIMS results of possible impurities in as-grown InGaAsN

The presence of possible contaminants H, O, C, Si, B in the as-grown GaInAsN sample was determined using SIMS. H contaminant is inevitable in gas source MBE growth; C and Si are ubiquitous dopants and these contaminants can also come from air, steel and diffusion pump oil vapor; B may present due to the BN present in the RF plasma source; and O contaminant is also possible from water vapor and the oxidation of materials. The results are shown in figure 8.3. It is clear that B is emitted from the RF source during its operation. The source of this B is from the BN from which the discharge chamber and the exit aperture plate are made. The measured B concentration is $6x10^{16}$ cm^{-3} and exceeds the background level by more than two orders of magnitudes. However, the concentration of B in the substrate (depth >1.05 μm) is even higher than $3x10^{18}$ cm^{-3}, which is characteristic of LEC grown GaAs wafers[71,72]. The concentration of O and H also increases slightly when the N-source is open such that a nitride is being grown. Si shows a very slight increase in concentration during the growth of nitride layer, and C exhibits no change in the nitride layer, compared to the background level.

In addition to the as-grown sample, an annealed GaInAsN sample was also analyzed by SIMS. The annealing condition was 700 ^{0}C for 1.5hr for the sample shown in figure 8.1. This is close to the optimum annealing condition we found for GaInAsN with low N concentration. The In and N concentrations in the GaInAsN layer are essentially the same as those of the as-grown sample, as shown in figure 8.4. The small deviation of the N and In concentrations from that of the as-grown sample is believed to be mainly due to the different SIMS sample pieces cut from different areas of the wafer, and the concentration profile was not perfectly uniform over the entire wafer. The N and In concentration distribution at the interface between the nitride layer and the nitrogen-free epitaxial layer are not significantly changed, and the interface was not significantly broadened due to annealing.

As for the possible contaminants H, O, C, Si, B, SIMS observation indicates they have different response to the annealing. C, Si, and B show no changes in their concentration in the annealed nitride layer in spite of a big diffusion tail observed for B (figures not shown here). However, H and O show some differences for the as-grown and annealed samples as shown in figure 8.5. The reduction of the H concentration in the nitride layer after annealing is expected, but the reduction of O in the nitride layer and the GaAs layer is unexpected and it was probably caused by changing the O calibration.

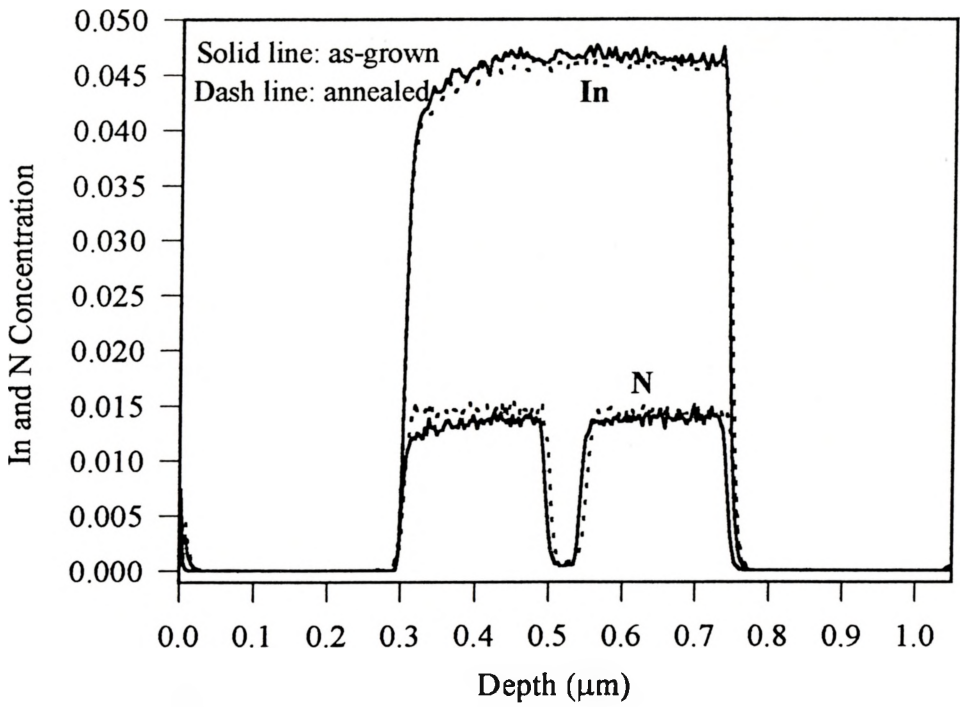

Fig.8.4 N and In concentrations for both annealed and as-grown samples in figure 8.1

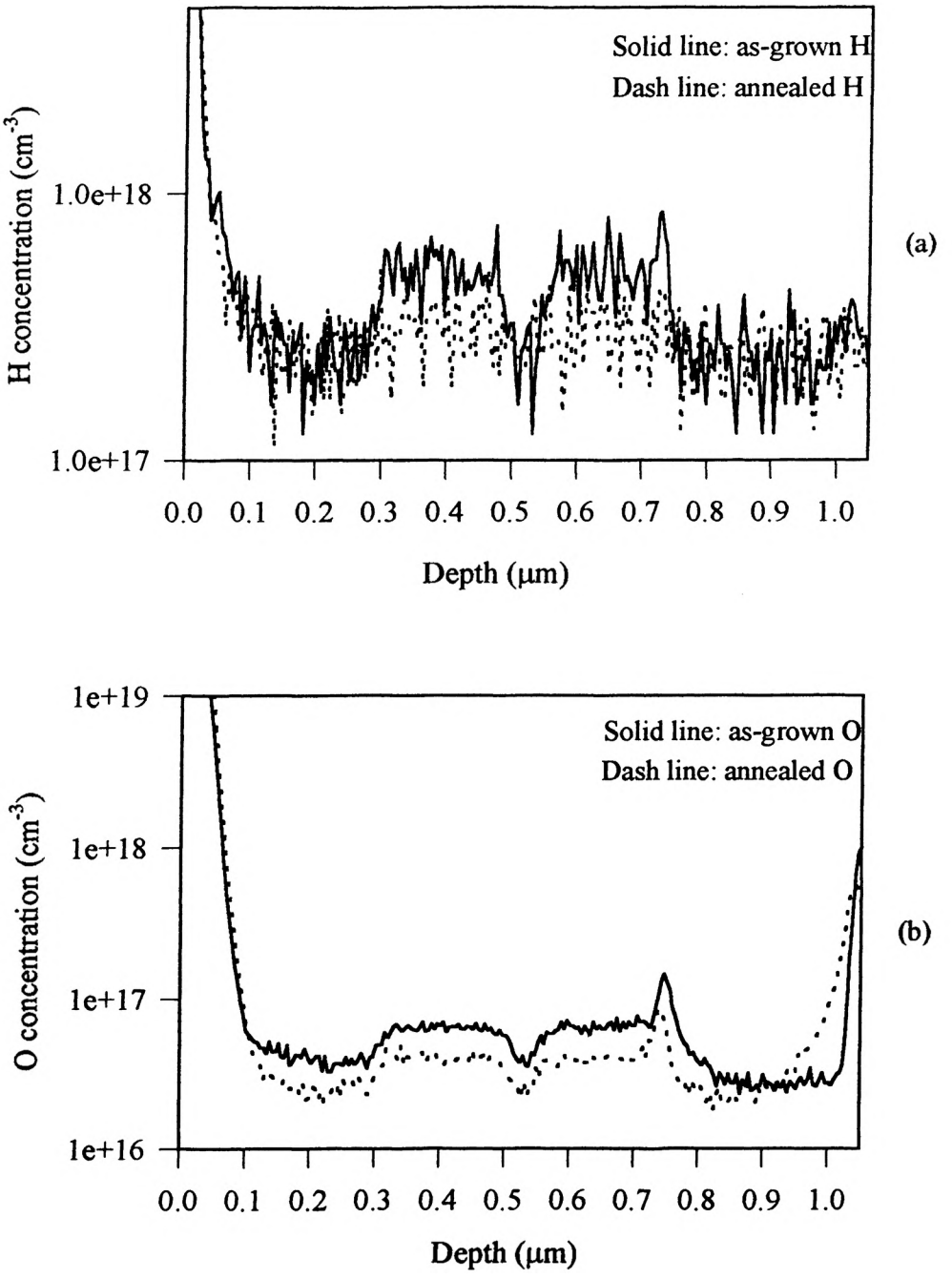

Fig.8.5 H and O concentration in both as-grown and annealed GaInAsN samples

The above SIMS observations will be correlated with Hall effect measurement results and further discussion will be provided in later this chapter.

8.2 Hall effect measurements of un-doped, Si-doped and Be-doped GaInAsN

The sample structures for Hall effect measurements are a $Ga_{0.955}In_{0.045}As_{0.985}N_{0.015}$ epitaxial layer, 1 or 2 μm thick, grown on a semi-insulating GaAs substrate. Un-doped, Si-doped (nominally $n=4x10^{17}$ cm^{-3}) and Be-doped (nominally $p=4x10^{17}$ cm^{-3}) layers were grown. In order to verify the reliability of the measurement data, comparative Hall effect measurements were also carried out on un-doped, Si-doped (nominally $n=4x10^{17}$ cm^{-3}) and Be-doped (nominally $p=4x10^{17}$ cm^{-3}) GaAs epitaxial layers of the same thickness as the $Ga_{0.955}In_{0.045}As_{0.985}N_{0.015}$ samples. In addition, the samples were measured after annealing at 725 ^{0}C for 30min. This is close to the optimum annealing condition found for GaInAsN.

The results of Hall effect measurements are summarized in table 8.1. Corrections for the depletion layer thickness have been included where possible. The corrections include surface and interface depletion corrections[66]. The carrier concentration of un-doped GaAs samples (~10^{15} cm^{-3}) is lower than that of doped samples by about 2 orders of magnitude. The corrected values for the surface and interface depletion layers are more precise at high doping and less precise at low carrier concentration levels. There are two values for un-doped GaAs samples in the table. The smaller value is the measured un-corrected value, which represents the lower limit of the carrier concentration, while the bigger value is the estimated carrier concentration after correcting for the surface

depletion layer and interface depletion layer. For the un-doped GaInAsN samples, the carrier concentrations in the table are estimates since the GaInAsN layer is fully depleted.

	Material	Doping	Thickness (μm)	Type	Carrier conc. (cm^{-3})	Mobility ($cm^2/v.s$)
As-grown	GaAs	undoped	2	p	$5.9x10^{14}$ ~$2.0x10^{15}$	450
	InGaAsN	undoped	2	n	$3.6x10^{11}$	480
	GaAs	Be	1	p	$3.8x10^{17}$	200
	InGaAsN	Be	1	p	$3.0x10^{16}$	150
	GaAs	Si	1	n	$4.0x10^{17}$	3600
	InGaAsN	Si	1	n	$3.0x10^{16}$	260
Annealed	GaAs	undoped	2	p	$6.7x10^{14}$ ~$2.0x10^{15}$	460
	InGaAsN	undoped	2	n	$5.7x10^{12}$	1680
	GaAs	Be	1	p	$3.7x10^{17}$	250
	InGaAsN	Be	1	p	$1.8x10^{17}$	170
	GaAs	Si	1	n	$3.9x10^{17}$	3700
	InGaAsN	Si	1	n	$1.8x10^{17}$	470

Table 8.1 Hall effect measurements of un-doped, Si-, Be-doped GaInAsN and GaAs

For the as-grown samples, the carrier concentration of un-doped GaInAsN is significantly smaller than that of un-doped GaAs. This phenomenon suggests the presence of defects acting as hole traps (deep donors) introduced along with the N incorporation. These hole traps compensate the low p-type background as found in GaAs

and force the Fermi level to be slightly above mid-gap resulting in a weakly n-type sample. The concentration of defects acting as a hole traps can be estimated from the Be-doped GaInAsN material. The nominal doping level of Be in GaInAsN is $4x10^{17}$ cm^{-3}, and is determined to be $3.8x10^{17}$ cm^{-3} in GaAs. The real measured carrier concentration in GaInAsN is only $p=3x10^{16}$ cm^{-3}. This suggests that the number of defects acting as hole traps is at least $3.5x10^{17}$ cm^{-3}. However, the actual number of traps is dependent of the energy level of the traps in the energy bandgap. Moreover, the same Hall effect measurement performed on Si-doped GaInAsN and GaAs indicates that the defects acting as electron traps (deep acceptors) also exist, and the number of the electron traps is estimated to be at least $3.7x10^{17}$ cm^{-3} depending on the energy level of the traps within the bandgap. The close value of the number of electron traps and hole traps might be coincidental. Further detailed analysis on more samples with different doping levels will be needed in the future to obtain reliable estimates of the concentration of electron and hole traps. The lower mobility of Si-doped GaInAsN compared to that of GaAs indicates the presence of a large concentration of defect scattering centers.

Hall effect measurements were also carried out on annealed GaInAsN and GaAs samples. The results are also shown in table 8.1. For the GaAs material, it is seen that, as expected, the carrier concentration and mobility are essentially the same for the annealed and as-grown samples no matter whether they are un-doped, Si-doped or Be-doped. However, for the GaInAsN epitaxial layer, the electrical properties show significant improvement after annealing. The general tendency of GaInAsN after annealing is an increase in the carrier concentration (about 5 times for the Si- and Be-doped material) and also an increase of mobility. However, hole and electron traps still remain. From the measured carrier concentration values of Si-doped and Be-doped GaInAsN and GaAs, the number of defects acting as hole traps and electron traps in the annealed GaInAsN sample

are at least $1.9x10^{17}$ cm^{-3} and $2.1x10^{17}$ cm^{-3}, respectively. These values are smaller than those of the as-grown samples. This is consistent with the PL measurement results where annealing of the GaInAsN samples results in greatly improved PL intensity, but they still display lower optical quality than the nitrogen-free InGaAs samples due to defects still present in GaInAsN epitaxial layer.

8.3 Discussion

A significant reduction in the optical and electrical qualities of GaInAs and GaAs is observed following the incorporation of a small amount of N as reported by other research groups[73-81]. Several mechanisms might be responsible for these degraded properties, such as phase separation, contaminant incorporation, and/or defect formation. In the following section, some discussions on these subjects are provided based on our observations from PL, TEM, SIMS, and Hall effect measurement results.

Due to the large difference of lattice constants of the binary constituents phase separation has been typically reported as the main reason responsible for the poor photoluminescence quality of GaInAsN[67,68]. Spinodal decomposition in GaInAsN was indeed observed in our TEM analysis. According to the detailed studies of spinodal decomposition in InGaAsP material[82,83], this phenomenon was responsible for a detrimental effect on the photoluminescence quality, producing a reduced PL intensity and broadening of the photoluminescence peak. However, annealing of samples with spinodal decomposition at annealing temperatures of 650^0C~800^0C did not significantly change the photoluminescence behavior since the thermal energy in this temperature range is not sufficient to overcome the energy barrier of spinodal decomposition[84]. By comparison, TEM studies performed on GaAsN epitaxial layers with a small N content

(N~1.74%) indicate no spinodal decomposition (see fig. 7.7). However, the photoluminescence intensity of GaAsN with a small N content is also much reduced compared to InGaAsN . These experimental results suggest that spinodal decomposition in GaInAsN is one possible explanation for the degradation of the PL intensity and the broadened PL peak, but it is not the key reason.

The main reason for the reduction of the PL intensity of GaInAsN is probably due to defects formed by impurities deriving from the operation of the nitrogen plasma source. Indeed, a high O impurity level (~10^{18} cm^{-3}) was reported in the MOCVD growth of GaInAsN[32], and authors suggested that O might act as a non-radiative recombination center. However, according to our SIMS results, the concentration of O in MBE-grown GaInAsN is only about $6.5x10^{16}$ cm^{-3}; only slightly higher than that of the background level of $4x10^{16}$ cm^{-3} in a GaAs layer. Therefore, O impurities do not play a significant role in the degradation of the optical quality of MBE-grown GaInAsN. From figure 8.3, the impurity level of B is clearly increased due to the operation of the RF N source. However, the concentration of B is still below $1x10^{17}$ cm^{-3}, also B is a group-III element and is expected to be electrically inactive. Most of B may just sit in the group III site in the material. The other two impurities Si and C, although they are electrically active, have very low concentrations of only about $3x10^{15}$ cm^{-3} and $2x10^{16}$ cm^{-3}, respectively. Such low concentrations can not account for the charge compensation effect in GaInAsN which is observed in Hall effect measurements. Therefore, the poor PL quality of GaInAsN can not be attributed to the impurities B, Si, and C. From the SIMS results shown in figure 8.3, the concentration of H in GaInAsN is about $2.5x10^{17}$ cm^{-3}, higher than that of the background level in GaAs. This excess H concentration is close to the value of the estimated defect concentration, although it could be just a coincidence. After annealing, the excess H concentration in GaInAsN is reduced significantly and this is

coincident with the improvement of PL intensity. N-H_2 complexes have been suggested as possible defects responsible for the poor optical quality of GaInAsN in MOCVD growth[31]. However, the mechanism by which this defect behaves is not currently known.

Energetic N_2^+ ions or excited N_2 molecules produced by the nitrogen plasma source might be another source of defects in nitride materials grown by MBE[38,34]. Some measures have been taken to reduce the ion density in the plasma, such as (1) use of an RF plasma source rather than an ECR plasma source, and (2) changing (reducing) the conductance aperture used in an RF source. These measures did somewhat improve the optical quality of the materials in this thesis work. However, the optical quality of nitrides is still not comparable to the nitride-free material. In comparison, GaInAsN and GaAsN grown using MOCVD, where the nitrogen plasma is not used, also exhibits poor optical quality. Thus the conclusion that defects caused by energetic N_2^+ ions in the plasma are the main reason responsible for the poor optical quality of nitrides is questionable. In order to establish the role of energetic plasma paticles, an InGaAs sample was grown under the same conditions as GaInAsN, with a He plasma generated by the RF source. Although He is chemically inactive and will not incorporate into the GaInAs material, it is expected that energetic He plasma particles will produce defects similar to the N plasma. However, the results indicate no reduction of the PL intensities between the GaInAs sample grown under He plasma and the reference GaInAs sample. This leads to the conclusion that the ion induced defects from the plasma are not the key reason responsible for the significant reduction of the PL yield of GaInAsN with a small amount of N incorporated.

Therefore, the introduction of defects into GaInAsN and GaAsN must come from the N incorporation process itself. As discussed earlier, the spinodal decomposition

occurring during the growth of GaInAsN at normal growth temperatures seems not to be the explanation for the dramatically decreased PL intensity of the nitride. One suggested possible reason is that N-N pairs formed on the growing surface cause a surface lattice distortion which then leads to point defects in the GaInAsN and GaAsN materials[63]. However, this is only the subjective guess, and its mechanism is unknown.

CHAPTER 9
Conclusion and suggested future works

Quaternary GaInAsN is a potentially promising material for realizing long wavelength emission lasers for use in optical communications systems. Such devices should have better high temperature characteristics than current InGaAsP lasers due to an increase of the conduction band offset. The GS-MBE growth of quaternary GaInAsN and ternary GaAsN were carried out in this work. Photoluminescence, X-ray diffraction, TEM, SIMS and Hall effect measurements were used to characterize thick layers and quantum wells of these nitride materials.

The concentration of N incorporated into GaInAs or GaAs is very dependent of growth conditions. Active N can be obtained by using either an RF plasma source or ECR plasma source. RF plasma source was found to produce better quality of nitride materials due to much reduced N_2^+ ion density and excited 2^{nd} molecular series in the plasma. The controlling factors in the operation of the RF plasma source are RF power and nitrogen flow. Growth conditions such as the substrate temperature,III/V flux ratio and As_2 flux also affect the amount of N incorporated. X-ray diffraction and photoluminescence measurements indicate that N incorporated into compressively strained InGaAs reduces the strain and produce a red-shift of photoluminescence peak. However, the optical quality is degraded producing a reduced photoluminescence intensity and broadening of PL peak. Therefore, the threshold current density of currently demonstrated GaInAsN laser diodes is higher than for conventional InGaAsP laser diodes[24,26], and the concentration of N used is limited to less than 1%.

Hall effect measurement suggests that there exist large number of hole and electron traps in the epitaxial GaInAsN. The defects formed in the materials seem not caused by the energetic N_2^+ ion damage, but result from the N incorporation process. Impurities such as O, Si, C, B except H are not responsible for degrading the optical quality, because their concentrations revealed by SIMS are at least one order of magnitude less than the estimated concentration of hole traps and electron traps determined by Hall effect measurement. Spinodal decomposition of GaInAsN was observed in TEM micrographs. It is one factor that may contribute to optical quality degradation, but is not the main reason responsible for quenching PL intensity in nitrides because no obvious phase separation was found for a GaAsN epitaxial layer where very poor optical quality was still observed. The possible key reason was attributed to the N incorporation process, such as N-N pair formed leading to point defects, but it is only subjective guess and its mechanism is unknown.

Some methods have been used to improve the optical quality of GaInAsN epitaxial layers. They include optimization of growth conditions and using post-growth annealing. Annealing was found an effective way to improve the optical quality. Annealing at 700 ^{0}C for more than 1 hr is the optimum annealing condition for the GaInAsN with N composition around 1%. The PL intensity could be increased up to 40 times compared to the as-grown material. The mechanism responsible for the annealing behavior is currently unknown.

From the results obtained to date, the following proposals for future works are made:

(1) The nature of defects is not currently clear for GaInAsN. More defect studies are needed to understand their nature and mechanism of introduction into GaInAsN. By

associating the introduction of defects with a specific growth process, it might be possible to minimize the defect introduction.

(2) The role of atomic N and 1st excited N_2 molecular series from nitrogen plasma source on the growth of nitride is not clear. More experiments on this subject are necessary so as to further improve nitride layer quality.

(3) Since annealing has been shown to be an effective method for improving the optical quality, more systematic annealing studies should be carried out to help understand the mechanism of annealing in GaInAsN.

(4) Very recently, using a flux of Sb during growth of GaInAsN was found to be effective at improving the optical quality[48]. X. Yang[48] suggested that Sb acts as a surfactant during growth which somehow produce a significant enhancement of the PL and laser performance. This process needs further study.

(5) To realize a practical laser emitting at 1.3μm, useful for telecommunication application, it is necessary to incorporate approximately 1.4% N into GaInAsN and the In content should be about 30%. This will allow a GaInAsN QW (70 Å thick) suitable for 1.3μm emission to be grown without strain relaxation. After the expitaxial GaInAsN layer reach certain good quality, the demonstrative experiments of fabrication and characterization of GaInAsN QW laser should be performed.

REFERENCES

1). M. Yano, H. Nishi and M. Tukusagawa, *J. Appl. Phys.* **52**, 3172, (1981)

2). G.B. H. Thompson and G. D. Henshall, *Electron. Lett.*, **16**, 42, (1980)

3). A. Haug, *Appl. Phys. Lett.*, **42,** 512, (1983)

4). A. Mozer, K.M. Romanerk, W. Schmid and M.H. Pilkuhn, E. Schlosser, *Appl. Phys. Lett.*, **15**, 964, (1982)

5). A.R. Adams, M.Asada, Y. Suematsu and S. Arai, *Jpn. J. Appl. Phys.* **19**, L621, (1980)

6). A.R. Adams, *Electron. Lett.*, ***22,*** 249, (1986)

7). C.E.Zah, R.Bhat, B.Pathak, F.Favire, W. Lin, M.C. Wang, N.C. Andreadakis, D.M. Hwang, M.A. Koza, T.P Lee, Z. Wang, D. Darby, D. Flanders, and J. J. Hsieh, *Electron. Lett., 27,* 1414, (1991)

8). M. Yamamoto, N. Yamamoto, and J. Nakano. *IEEE J. Quantum Electron*, **30**, 554, (1994)

9). M. Kondow, K.Uomi, A. Niwa, and T.Kitatani, *Jpn. J. Appl. Phys.* ***35,*** 1273, (1996)

10). K. Nakahara, M. Kondow, T. Kitatani, Y. Yazawa, and K. Uomi, *Electron. Lett.*, **32**, 1585, (1996)

11). K. Nakahara, M. Kondow, T. Kitatani, M.C. Larson and K. Uomi, *IEEE Photon. Technol. Lett.*, **10**,487, (1998)

12). M.C. Larson, M. Kondow, T. Kitatani, K. Nakahara, *IEEE Photon. Technol. Lett.*, **10**, 188, (1998)

13).S.R.Kurtz, A.A. Allerman, E.D.Jones, J.M. Gee, J.J. Banas, and B.E. Hammons, *Appl. Phys. Lett.*, **74,** 729, (1999)

14). D.J. Friedman, J.F. Geisz, S.R. Kurtz, J.M. Olson, *J. Crystal Growth*, **195**,409, (1998)

15). H. P. Xin and C. W. Tu, *Appl. Phys. Lett.*, **75**, 1416, (1999)

16). Z.Pan, T.Miyamoto, D. Schlenker, F. Koyama and K. Iga, *Jpn. J. Appl. Phys.* **38**, 1012, (1999)

17). G.B. Stringfellow, *J. Electrochem. Soc.*, **119**, 1780, (1972)

18). Y. Qiu, S.A. Nikishin, H. Temkin, V.A. Elyukhin, and Y. A. Kudriavtsev, *Appl. Phys. Lett.*, **70**, 2831, (1997)

19). H. P. Xin and C. W. Tu, *Appl. Phys. Lett.*, **72**, 2442, (1999)

20). T. Kitatani, M. Kondow, K. Nakahara, M.C. Larson, Y. Yazawa, M. Okai, K. Uomi, *J. Crystal Growth,* **201/202**, 351, (1999)

21). T.Miyamoto, K. Takeuchi, T. Kageyama, F. Koyama and K.Iga, *J. Crystal Growth,* **197**, 67, (1999)

22). N.Y. Li, C.P. Hains, K. Yang, J.Lu and J.Cheng, *Appl. Phys. Lett.*, **75**, 1051, (1999)

23). S. Sakai, Y. Ueta, and Y. Terauchi., *Jpn. J. Appl. Phys.* **32**, 4413, (1993)

24). M. Kondow, T. Kitatani, S. Nakatsuka, M.C. Larson, K. Nakahara, Y. Yazawa, M. Okai, and K. Uomi, *IEEE J. of selected topic in Quantum Electronics*, **3**, 719, (1997)

25). A. Ougazzaden, Y. Le. Bellego, E.V.K. Rao, *Appl. Phys. Lett.*, **70**, 2861, (1997)

26). N.Y. Li, C.P. Hains, K, Yang, J. Lu, J. Cheng, P.W. Li, *Appl. Phys. Lett.*, **75**, 1051, (1999)

27). W.G. Bi and C. W. Tu, *Appl. Phys. Lett.*, **72**, 1161, (1998)

28). Z.Pan, T.Miyamoto, D. Schlenker, F. Koyama and K. Iga, *J. Appl. Phys.* **84**, 6409, (1998)

29). T. Kageyama, T. Miyamato, S. Makino, *Jpn. J. Appl. Phys.*, **38** (pt.2), L298, 1999

30). H.P.Xin, K.L. Kavanagh, M. Kondow, C.W. Tu, *J. Crystal Growth*, **201/202**, 419, (1999)

31). E.V.K. Rao, A. Ougazzaden, Y. Le Bellego, M. Juhel, *Appl. Phys. Lett.*, **72**, 1409, (1998)

32). R. Bhat, C. Caneau, L. S. Riba, W. Bi, C. Tu, *J. Crystal Growth*, **195**, 427, (1998)

33). O.M. Khreis, K.P. Homewood, W.P. Gillin, and K.E.Singer, *J. Appl. Phys.* **84**, 4017, (1998)

34). T. Kageyama, T.Miyamoto, S. Makino, F. Koyama and K.Iga, *Workbook of ICCBE-7*, Tsukuba, Japan, Th4-1, (1999)

35). O.M. Khreis, W.P. Gillin, and K.P. Homewood, *Phys. Review*, **B55**, 15813, (1997)

36). J.W. Mattews, and A.E. Blakeslee, *J. Crystal Growth*, **27**, 118, (1974)

37). M. Kondow, K.Uomi, K.Hosoni and T. Mozume, *Jpn. J. Appl. Phys.* **33**, L1056, (1994)

38). W.C.Hughes, W.H.Rowland, Jr., M.A.L. Johnson, S. Fujita, J.W. Cook Jr., J.F. Schetzina, J.Ren, and J.A. Edmond, *J. Vac. Sci. Technol.* **B13**, 1571, (1995)

39). R. J. Monlnar, R. Singh, and T.O. Moustakas, *Appl. Phys. Lett.*, **66**, 268, (1995)

40). M.E. Lin, B. Sverdlov, G.L. Zhou, and H. Morkov, *Appl. Phys. Lett.*, **62**, 3479, (1993)

41). G.B. Stringfellow, *J. Appl. Phys.*, **43**, 1249, (1972)

42). J.C.Philips, *Phys. Lett.*, **20**, 550, (1968)

43). J.A. Van Vechten, *Phys. Rev.*, **170**, 773, (1968)

44). J.W. Cahn, *Acta Metallurgica*, **9**, 795, (1995)

45). J.L. Lazzari, E. Tournie, F. Pitard, and A. Joullie, *Mater. Sci. Eng.*, **B9**, 125, (1991)

46). L. Bellaiche, S.H. Wei, and A. Zunger, *Appl. Phys. Lett.*, **70**, 3558, (1997)

47). S. Francoeur, G. Sivaraman, Y. Qiu, Appl. *Phys. Lett.*, **72**, 1857, (1998)

48). X.Yang, M.J. Jurkovic, J.B. Heroux and W.I. Wang, *Appl. Phys. Lett.*, **75**, 178, (1999)

49). R.W.B. Pearse, and A.G. Gardon, *The Indentification of Molecular Spectra*, Wiley, New York, P.209-220, (1963)

50). A.N. Wright, and C.A. Winkler, *Active Nitrogen*, Academic, New York, P.13-82, (1968)

51). A.T. Macrander, and S. Lau, *J. Electrochem. Soc.*, **138**,1147, (1991)

52). Y.P. Varshini, *Physica*, **A34**, 149, (1967)

53). A. Katz, *Indium Phosphide and Related Materials*, Artech House Inc., P.45-73, (1992)

54). L.J. Vander Pauw, *Philips Res. Repts.*, **13**, 1, (1958)

55). E.F. Schubert, *Cambridge Studies in Semiconductor Physics and Microelectronic Engineering*: **1**, University Press, London, P.482-487, (1993)

56). H. Saito, T. Makimoto, and N. Kobayashi, *J. Crystal Growth*, **195**, 416, (1998)

57). S. Adachi, *J. Appl. Phys.*, **53**, 8775, (1982)

58). S.L. Chuang, *Phys. Rev.* **B, 43**, 9649, (1991)

59). T.D. Moustakes, *Semiconductors and Semimetals*, **57**, chapter 2, 33, (1999)

60). T. Miyamoto, K. Takeuchi, T. Kageyama, F. Koyama, and K. Iga, *J. Crystal Growth*, **197**, 67, (1999)

61).W.G. Bi, C.W. Tu, *J. Crystal Growth*, **175/176**, 145, (1997)

62).W.G. Bi, C.W. Tu, *J. Appl. Phys.*, **80**, 1934, (1996)

63). B. Robinson, Lixiang Yuan, D.A. Thompson, S.A. McMaster, R.W. Streater, *Photonics Taiwan: Optoelectronic material and device II*, July 26, 2000, *Proceedings of SPIE*, **4078**, (2000)

64). H.P.Xin, K.L. Kavanagh, C.W. Tu, *J. Crystal Growth*, **208**, 145, (2000)

65). T. Okada, Ph.D dissertation, *Growth related phenomena in MBE films on InGaAsP on InP substrates*, McMaster University (1996)

66).A. Chandra, C.E.C. Wood, D.W. Woodard and L.F. Eastman, *Solid State Electron.* **22**, 645, (1979)

67). J.W. Orton, D.E. Lacklison, N.Baba-Ali, C.T. Fox, T.S. Cheng, S.V. Novikov, D.F.C. Johnston, S.E. Hooper, L.C. Jenkins, L.J. Challis, and T.L. Tansley, *J. Electron. Mater.*, **24**, 263, (1995)

68). H.P.Xin, K.L. Kavanagh, Z.Q. Zhu, and C.W. Tu, *Appl. Phys. Lett.*, **74**, 2337, (1999)

69). D.Schlenker, T.Miyamato, Z. Pan, F. Koyama, and K.Iga, *J. Crystal Growth*, **196**, 67, (1999)

70). I.Ho and G.B. Stringfellow, *J. Crystal Growth*, **178**, 1, (1997)

71). I.C. Bassignama, D.A. Macquistan, G.C. Hiller, R. Streater, D. Beckett, A. Majeed, and C. Miner, *J. Crystal Growth*, **178**, 445, (1997)

72). I.C. Bassignama, D.A. Macquistan, R. Streater, G.C. Hiller, G.C. Hiller, R.Packwood, and V. Moore, *J. Crystal Growth*, **172**, 25, (1997)

73). M. Kondow, T. Kitatani, M.C. Larson, K. Nakahara, K. Uomi, and H. Inoue, *J. Crystal Growth*, **188**, 255, (1998)

74).T. Kageyama, M. Kondow, S. Nakatsuka, Y. Yazawa and M. Okai, *IEEE J. of Selected Topics in Quant. Electron.*, **3**, 206, (1997)

75).W.G. Bi, Y.Ma, J.P. Zhang, L.W. Wang, S.T.Ho, and C.W.Tu, *IEEE Photon. Tech. lett.*, **9**, 1072, (1997)

76). M. Kondow, K. Uomi, T. Kitatani, S. Watahiki, Y. Yazawa, *J. Crystal Growth*, **164**, 175, (1996)

77). C.F. Foxon, T.S. Cheng, S.V. Novikov, *J. Crystal Growth*, **150**, 892, (1995)

78). K. Uesugi, N. Morooka, and I. Suemune, *J. Crystal Growth*, **201**, 355, (1999)

79). A.F. Wright and J.S. Nelson, *Appl. Phys. Lett.* **66**, 3051, (1995)

80). W.E. Hoke, P.J. Lemonias, and D.G. Weir, *J. Crystal Growth*, **111**, 1024, (1991)

81). L. Grenouillet, C. Bru-Chevallier, G. Guillot, P. Gilet, P. Duvaut, C. Vannuffel, A. Million, and A. Chenevas-Paule, *Appl. Phys. Lett.* **76**, 2241, (2000)

82). R.R. Lapierre, T. Okada, B.J. Robinson, D.A.Thompson, G.C. Weatherly, *J. Crystal Growth*, **158**, 6, (1996)

83). R.R. Lapierre, B.J. Robinson, D.A.Thompson, *Appl. Surface Sci.*, **90**, 437, (1995)

84). R.R. Lapierre, private communication, 1999